frontiers | Frontiers in Marine Science

ORIGINAL RESEARCH
published: 30 June 2022
doi: 10.3389/fmars.2022.878116

Coupled Oceanic and Atmospheric Controls of Deglacial Southeastern South America Precipitation and Western South Atlantic Productivity

Karl J. F. Meier[1], Andrea Jaeschke[2], Janet Rethemeyer[2], Cristiano M. Chiessi[3], Ana Luiza S. Albuquerque[4], Vincent Wall[2], Oliver Friedrich[1] and André Bahr[1]*

[1] Institute of Earth Sciences, Heidelberg University, Heidelberg, Germany, [2] Institute of Geology and Mineralogy, University of Cologne, Cologne, Germany, [3] School of Arts, Sciences and Humanities, University of São Paulo, São Paulo, Brazil, [4] Programa de Geociências (Geoquímica), Universidade Federal Fluminense, Niterói, Brazil

OPEN ACCESS

Edited by:
Ed Hathorne, Helmholtz Association of German Research Centres (HZ), Germany

Reviewed by:
Li Lo, National Taiwan University, Taiwan
Pepijn Bakker, VU Amsterdam, Netherlands
Daniel Gebregiorgis, Georgia State University, United States

***Correspondence:**
Karl J. F. Meier
karl.meier@geow.uni-heidelberg.de

Specialty section:
This article was submitted to Marine Biogeochemistry, a section of the journal Frontiers in Marine Science

Received: *17 February 2022*
Accepted: *26 May 2022*
Published: *30 June 2022*

Citation:
Meier KJF, Jaeschke A, Rethemeyer J, Chiessi CM, Albuquerque ALS, Wall V, Friedrich O and Bahr A (2022) Coupled Oceanic and Atmospheric Controls of Deglacial Southeastern South America Precipitation and Western South Atlantic Productivity. Front. Mar. Sci. 9:878116. doi: 10.3389/fmars.2022.878116

Various mechanisms were proposed as substantial drivers of (sub)tropical South American hydroclimate changes during the last deglaciation. However, the interpretation of past precipitation records from the regions affected by the South American Summer Monsoon, the dominant hydroclimatic system in (sub)tropical South America, still insufficiently consider feedbacks between oceanic and atmospheric processes evident in modern observational data. Here, we evaluate ocean-atmosphere feedbacks active in the region from 19 to 4 ka based on a multi-proxy record comprising lipid biomarker, bulk sediment elemental composition and foraminiferal geochemistry from a sediment core retrieved from the tropical western South Atlantic offshore eastern Brazil at ~22°S. Our proxy data together with existing paleoclimate records show that the consideration of large scale synoptic climatic features across South America is crucial for understanding the past spatio-temporal rainfall variability, especially during the last deglaciation. While the paleohydrological data from our study site show relatively stable precipitation across the deglaciation in the core region of the South Atlantic Convergence Zone, distinct hydroclimatic gradients developed across the continent during Heinrich Stadial 1, which climaxed at ~16 ka. By then, the prevalent atmospheric and oceanic configuration caused more frequent extreme climatic events associated with positive rainfall in the northern portion of eastern South America and in the southeastern portion of the continent. These climatic extremes resulted from substantial warming of the sub (tropical) western South Atlantic sea surface that fostered oceanic moisture transport towards the continent and the reconfiguration of quasi-stationary atmospheric patterns. We further find that enhanced continental precipitation in combination with low glacial sea level strongly impacted marine ecosystems *via* enhanced terrigenous organic matter input in line with augmented nutrient release to the ocean. Extreme rainfall events similar to those that occurred during Heinrich Stadial 1 are likely to recur in South America as a

consequence of global warming, because the projected reduction of the intra-hemispheric temperature gradient may lead to the development of atmospheric patterns similar to those in force during Heinrich Stadial 1.

Keywords: organic/inorganic geochemistry, South American Monsoon System, land-ocean teleconnection, South Atlantic Convergence Zone, last deglacial and holocene, South American Low Level Jet

INTRODUCTION

Past precipitation records from (sub)tropical South America highlighted that on orbital timescales, precipitation associated to the South American Monsoon System (SAMS) and South Atlantic Convergence Zone (SACZ), which is a particular feature of the SAMS, was mainly controlled by austral summer insolation. High (low) insolation lead to increased (decreased) moisture convection across the Amazon basin, which in turn increases (decreases) moisture export towards the southeast, seasonally feeding the SACZ and resulting in increased (decreased) SAMS rainfall over most parts of South America (Cruz et al., 2005; Hou et al., 2020). However, millennial-scale variations in South American precipitation during the last deglacial, such as Heinrich Stadial 1 (HS1) were driven by a different global climate forcing: induced by high-latitude forcing, the reorganization of cross-equatorial heat transport resulted from a marked slowdown of the AMOC leading to diminished oceanic heat export into the Northern Hemisphere. In turn, the distinct bi-polar distribution of heat in the Atlantic Ocean was expressed by simultaneous cooling of the northern and warming of the southern hemispheric sectors of the Atlantic Ocean. This global redistribution of heat had a determining influence on the latitudinal position and strength of atmospheric convection belts over the tropical Atlantic and affected the latitudinal position of the Intertropical Convergence Zone (ITZC). The southward shift of the ITCZ results from increased northward atmospheric heat transport into the colder hemisphere during phases of weak AMOC that is necessary to compensate the interhemispheric heat imbalance, and is in line with an intensification and a cross-equatorial extension of the Northern Hemisphere Hadley-Cell (Donohoe et al., 2012; McGee et al., 2014; Mulitza et al., 2017). Past studies indeed show a direct influence on moisture availability across South America by southward shifts of the ITCZ during periods of weak AMOC, which are, however, confined to the SAMS region in northern South America (Zhang and Delworth, 2005; Deplazes et al., 2013; Zhang et al., 2017; Bahr et al., 2018).

Southward shifts of the ITCZ and the associated adjustment of moisture flux pathways across tropical South America were further invoked to indirectly affect precipitation in the realm of the SACZ (Wang et al., 2007; Kanner et al., 2012; Stríkis et al., 2015; Stríkis et al., 2018). The latter studies implied that the deglacial high-latitude forced climatic perturbations and concomitant southward ITCZ shifts further boosted SACZ strength, thereby favoring moisture transport towards tropical and subtropical South America. However, Campos et al. (2019) revealed that precipitation anomalies in E and SE Brazil during phases of rapid climatic perturbations during the last deglaciation, i.e. HS1, were related to enhanced moisture flux from the tropical South Atlantic rather than SACZ intensification as suggested by prior studies. Further, variability in strength and extension of the SACZ, which determines precipitation in SE Brazil, is independent of a direct influence by the ITCZ. Instead, the SACZ strength appears to rather depend on synoptic climatic features across the Southern Hemisphere (Vera et al., 2002; Liebmann et al., 2004; Marengo et al., 2004; Silva and Berbery, 2006; Gelbrecht et al., 2018). Gelbrecht et al. (2018), for instance, found that eastward propagating atmospheric Rossby waves were the main driver of SACZ variability. The Rossby wave train determines the position of cyclonic and anticyclonic circulation across South America and the South Atlantic, which dominates the moisture flux towards the realm of the SACZ and subtropical South America. Yet, the ITCZ was found to play an indirect role in the synoptic atmospheric configuration in the Southern Hemisphere as southward shifts of the ITCZ weaken (invigorate) the strength of the subtropical (mid-latitude) jet, hence affecting the Southern Hemisphere Rossby wave train (Lee et al., 2011; Ceppi et al., 2013).

Since such synoptic climatic features were not considered in past paleo-precipitation studies from South America, the variability of SACZ-related precipitation and its controlling mechanisms during phases of rapid climatic perturbations during the last deglaciation such as during HS1 are not well constrained yet. Further, existing high-resolution SACZ reconstructions covering the last deglaciation are primarily based on terrestrial climate archives such as speleothems (Cruz et al., 2006; Cruz et al., 2007; Stríkis et al., 2015; Stríkis et al., 2018), while climate reconstructions from the core region of the SACZ based on marine sediment archives are still sparse (Campos et al., 2019).

Here we present a multiproxy record of marine sediment Core M125-35-3 collected off SE Brazil close to the Paraíba do Sul River mouth, whose catchment drains the core region of the modern SACZ (**Figure 1**). Thus, Core M125-35-3 is ideally located to reconstruct changes in the extension and intensity of the SACZ, its impact on the regional environment and the connectivity between SACZ and oceanographic changes during the last deglaciation. Our focus lies on the most intense phase of the interhemispheric seesaw during HS1 at ~16 ka which is captured by a high, sub-centennial-scale temporal resolution (in average ~57 yr). We first evaluate the capacity of the utilized inorganic and organic geochemical proxies to capture continental hydroclimate changes and their impact on terrestrial and marine environments. Then we discuss our

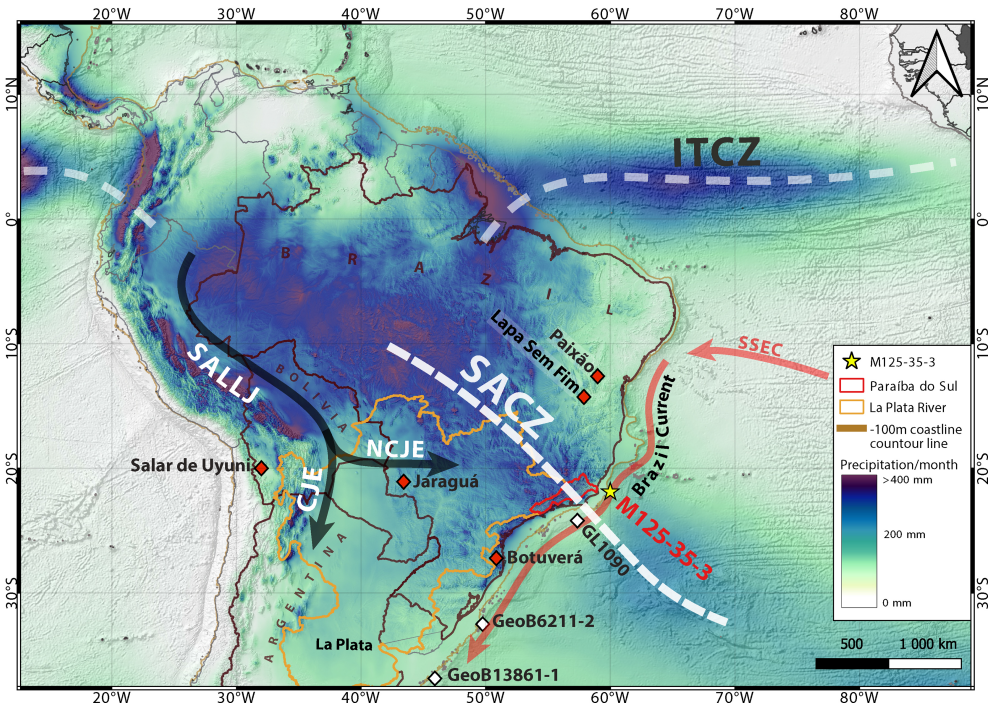

FIGURE 1 | Map of monthly average austral summer precipitation (December-February) across (sub)tropical South America (Karger et al., 2021). The precipitation pattern illustrates a fully established South American Monsoonal System. Note enhanced precipitation along the South Atlantic Convergence Zone (SACZ) indicated by NW-SE oriented white dashed line. The yellow asterisk marks Core M125-35-3 (this study). White diamonds indicate marine sedimentary climate archives mentioned in the text. Red diamonds reflect terrestrial paleo-rainfall reconstructions mentioned in the text. Black arrows indicate the South American Low Level Jet (SALLJ) in two different modes: the southward oriented Chaco Jet Event (CJE) and the eastward oriented No Chaco Jet Event (NCJE). The red and orange outlines indicate the drainage basins of the Paraíba do Sul located in the core region of the SACZ and the La Plata River. Countries mentioned in the main text (i.e. Brazil, Bolivia and Argentina) were outlined. The thick orange arrows represent major oceanic surface currents in the western sub(tropical) South Atlantic, namely the southward flowing Brazil Current which is fed by the southern South Equatorial Current (SSEC). ITCZ, Intertropical Convergence Zone.

findings in the context of large-scale atmospheric and oceanic fluctuations. We highlight that past precipitation variability and associated river run-off had a great influence on nutrient availability and marine productivity in the western tropical South Atlantic. Yet, the quantity of terrestrial influx to our study site is largely determined by the shelf extension and only subordinately controlled by precipitation intensity. Further we find that deglacial variability in the SAMS/SACZ system depends on a complex interplay of atmospheric and oceanographic processes on hemispheric scales. Unexpectedly, the spatial precipitation pattern reconstructed for glacial background conditions during HS 1 resembles modern observations and numerical model scenarios of future anthropogenic climate change under rising greenhouse gas concentrations (Gonzalez et al., 2013; Vera and Díaz, 2015; Saurral et al., 2017; Masson-Delmotte et al., 2021). Thus, improving our understanding of the response of the SAMS to climatic perturbations is instrumental in order to more reliably project how the spatial distribution and intensity of rainfall events might develop in response to global warming. This does not only relate to the socio-economic impacts of water shortage or flooding on the continent but must also consider the potential impact of marked changes in the hydrological cycle on coastal marine ecosystems.

OCEANOGRAPHIC AND CONTINENTAL SETTING

The Brazilian margin in the western tropical South Atlantic is dominated by the southward flowing Brazil Current (BC), which is the western boundary current of the South Atlantic subtropical gyre carrying warm tropical and oligotrophic waters of the Southern South Equatorial Current (SSEC) (Peterson and Stramma, 1991) (**Figure 1**). The BC flows southwards along the Brazilian margin from ~10°S as far as ~38°S where it converges with the northward-flowing cold Malvinas Current (MC) (Stramma and England, 1999) (**Figure 1**).

For the discussion of continental climate variability, we define the following geographic regions (**Figure 1**): (i) eastern South America (ESA) is defined as the region between ~10 and 20°S along the coastal realm of Brazil; (ii) southeastern South America (SESA) describes the region of Brazil south of 20°S including the Paraíba do Sul catchment; (iii) southern southeastern South America (SSESA), i.e. the region south of 30°S downstream the Paraná River and comprising the La Plata catchment (**Figure 1**).

Since we defined SESA as the region between ~20° and ~30°S it represents a transitional zone between tropical and subtropical climate features. During austral summer, modern precipitation

over SESA is dominated by the seasonal expansion and intensification of the SAMS/SACZ, which influence is greatest in the northern part of SESA in the core region of the SACZ including the Paraíba do Sul catchment (**Figure 1**). During austral winter, rainfall is related to mid-latitude cyclonic activity over the South Atlantic (Vera et al., 2002), affecting the Paraíba do Sul catchment less intensively than the southern part of SESA. With the onset of SAMS activity during austral summer, increased summer insolation enhances convection over tropical South America which induces increased moisture flux towards the continent in line with prevailing NE trade winds. The moist air is transported southward resulting in strong precipitation in the SACZ (Gan et al., 2004). The SACZ is a convective belt that extends from the Amazon basin southeastward into the western South Atlantic (Marengo et al., 2004).

Precipitation across ESA gradually decreases northward. In the southern part of ESA, which is closer to the NW-SE axis of the SACZ, precipitation seasonally increases in line with SAMS activity. Although SE trade winds continuously bring moisture towards the eastern headlands of Brazil, the hinterland region is characterized by a marked dry season during austral winter (Rao et al., 1993; Garreaud et al., 2009). The dry season becomes more extreme towards the semi-arid northeastern Brazil where an intensification of the Hadley Cell and descending convective motion of the Walker circulation results in increased aridity (Moura and Shukla, 1981; Ambrizzi et al., 2004; Garreaud et al., 2009; Marengo et al., 2017).

Seasonal variability in rainfall amounts across SSESA is weak. During austral summer, the coastal realms of SSESA receive increased rainfall when the SACZ is connected with the area of convection over the Amazon basin (Liebmann et al., 1999). During the SAMS season, the La Plata basin (including the Paraná catchment) receives large amounts of tropical moisture, when a northerly low-level flow is channeled east of the Andes and feeds convective storms over the subtropical plains (Saulo et al., 2000; Saulo et al., 2004; Marengo et al., 2004; Garreaud et al., 2009). This flow is known as the South American Low Level Jet (SALLJ), which we describe in more detail in section 5.3 (**Figure 1**). During austral winter, the main source of precipitation is frontal rainfall caused by incursions of sub-Antarctic cold fronts meeting tropical air masses (Vera et al., 2002; Garreaud et al., 2009).

The above described average precipitation pattern across South America may be disrupted by annual to multi-decadal climate phenomena (for a recent summary cf. Zanin and Satyamurty (2020)). Most importantly, a consistently described climate phenomenon is the occurrence of a tropical to subtropical precipitation dipole between the SAMS region influenced by the SACZ comprising the Paraíba do Sul catchment in SESA on the one hand and SSESA in the exit region of the SALLJ on the other hand (Nogués-Paegle and Mo, 1997; Robertson and Mechoso, 2000; Doyle and Barros, 2002; Díaz and Aceituno, 2003; Liebmann et al., 2004; Grimm, 2011; Boers et al., 2014; Grimm and Saboia, 2015; Jones and Carvalho, 2018; Zanin and Satyamurty, 2020). It is noteworthy that the SALLJ appears in two different configurations (**Figures 1**, **2**) (Salio and Nicolini, 2006): (i) the Chaco Jet Event (CJE); and (ii) the No Chaco Jet Event (NCJE). A main difference between those jet events is the meridional extension of the jet. Both jet events are channeled towards the southeastern portion of South America. The CJE, however, shows a maximum southward wind component above central Bolivia and continues northern Argentina. Instead, the NCJE protrudes eastward around 25°S, fostering moisture transport towards the SACZ at similar latitudes (Salio et al., 2002; Salio and Nicolini, 2006; Ramos et al., 2019) (**Figure 2**). This dipole pattern arises from the midlatitude Rossby wave train progressing eastward from the South Pacific Ocean and turns equatorward as it crosses the Andes Mountains. The prevalent mode of the SALLJ seems to be determined by the phase of the Rossby wave as it crosses the Andes Mountains and strongly modulates the upper and lower atmospheric circulation pattern across South America, in particular the circulation pattern and intensity of the SALLJ (**Figures 1**, **2**) (Vera et al., 2002; Liebmann et al., 2004; Vera et al., 2006; Silva and Berbery, 2006). Accordingly, a dipole pattern is determined by moisture flux carried during CJE (NCJE), leading to enhanced (decreased) precipitation over SSESA and dryer (wetter) conditions in the core region of the SACZ in SESA. Further, the negative dipole pattern has been linked to teleconnections associated with cooling of the North Atlantic, which leads to a southward shift of the ITCZ and enhanced cross-equatorial moisture flux over northwestern South America, finally feeding the northerly SALLJ in its CJE configuration during a negative SACZ/SALLJ dipole mode (Jones and Carvalho, 2018; Zanin and Satyamurty, 2020) (**Figure 2**). A positive SACZ/SALLJ dipole configuration operates the opposite way. The SACZ/SALLJ dipole appears to evolve as a feedback to changes in the spatial configuration of sea-surface temperatures (SST) in the western South Atlantic: a negative (positive) SACZ/SALLJ dipole is associated with warming (cooling) north (south) of 30°S (Venegas et al., 1997; Robertson and Mechoso, 2000; Doyle and Barros, 2002; Chaves and Nobre, 2004; Marengo et al., 2004; Garreaud et al., 2009). The spatial SST pattern, in particular warming of the western (sub)tropical South Atlantic north of 30°S, is fostered by radiative forcing after strengthening of the South Atlantic subtropical high above SESA induced by a stationary Rossby wave (**Figure 2**) (Robertson and Mechoso, 2000; Grimm and Ambrizzi, 2009; Grimm, 2011; Zanin and Satyamurty, 2020). This atmospheric configuration determines the exit region of the SALLJ, which corresponds to the CJE configuration: Atmospheric blocking by the persistent anticyclone diminishes easterly moisture flux during NCJE and reinforces northerly moisture flux towards SSESA *via* the CJE (**Figures 1**, **2**). This configuration could cause extreme weather events with marked droughts in the SACZ domain and floods in SSESA such as during the year 2014 as the SALLJ provides significant Amazon moisture export towards SSESA (Coelho et al., 2016) (**Figure 2**).

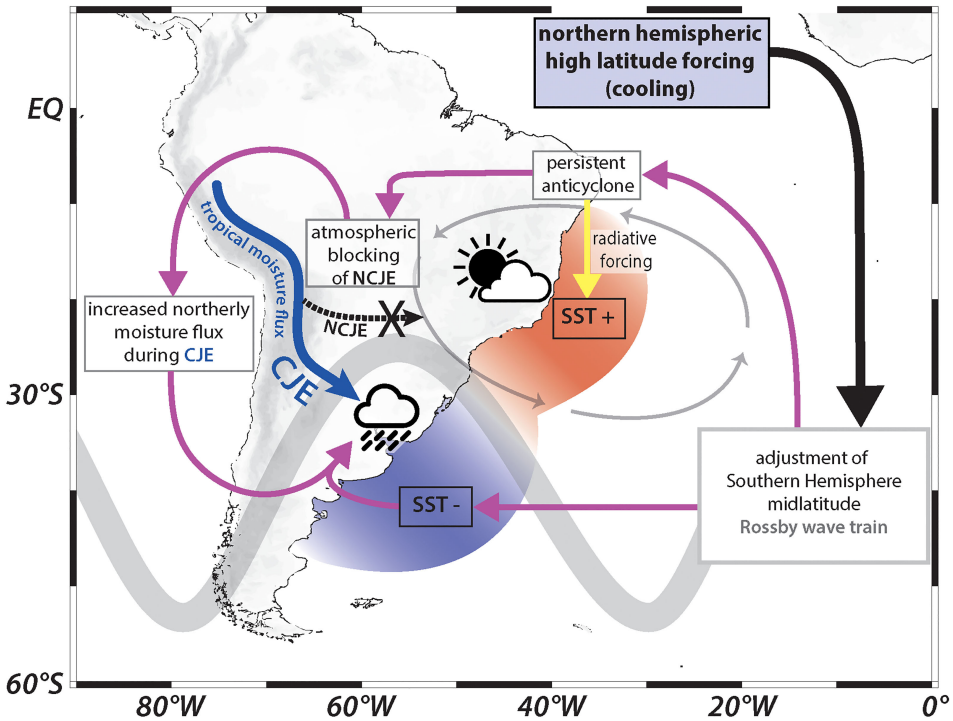

FIGURE 2 | Schematic representation of the mechanism active during the negative SALLJ/SACZ dipole phase in South America and the western South. Northern hemispheric cooling (in line with a southward shift of the ITCZ into the warmer Southern Hemisphere) triggers the adjustment of the Southern Hemisphere mid-latitude Rossby wave train (thick grey line). In turn, a persistent anticyclone (grey ellipse) establishes over eastern and southeastern Brazil. Increased radiative forcing (yellow arrow) leads to increased sea surface temperatures (SST) in the tropical western South Atlantic. The persistent anticyclone blocks the easterly flow of the SALLJ during its "non Chaco Jet Event" (NCJE) configuration (black dotted arrow) and prohibits tropical moisture flux towards southeastern South America (SESA). This results in dryer conditions across SESA. Tropical moisture is rather channeled by the SALLJ towards subtropical southern Southeastern South America during the "Chaco Jet Event" (CJE) (thick blue arrow), wich significantly increases rainfall in its exit region.

MATERIALS AND METHODS

Gravity core M125-35-3 was retrieved from the upper continental slope (21°53.606'S, 040°00.279'W, 428.6 m water depth), ~100 km off the Paraíba do Sul River mouth in SE Brazil during R/V Meteor cruise M125 in 2016 (Bahr et al., 2016). A total of 4.25 m of sediment was recovered. For lipid biomarker and bulk sediment elemental composition analyses, 89 sediment samples were taken downcore along the study interval between 25 and 170 cm covering the interval between 4 and 19 ka. Sample spacing for lipid biomarker and elemental analyses was not equidistant (in average ~1.5 cm) and adjusted to changing sedimentation rates in Core M125-35-3 to generate a temporally evenly resolved record. For foraminiferal geochemical analyses, the core was sampled between 25 and 170 cm at 1 cm spacing. Sampling was performed on the split-core working half of Core M125-35-3 using 10 cm^3 syringes at Universidade Federal Fluminense in Niterói, Brazil.

Lipid Biomarker Analysis

For biomarker analysis, sediment samples from Core M125-35-3 were freeze-dried and homogenized using an agate mortar. Samples (ca. 7 g) were ultrasonically extracted using a 2:1 mixture of dichloromethane (DCM) and methanol (MeOH), repeated 3 times. The extracts were combined and the solvent was subsequently removed by rotary evaporation under vacuum. The resulting total lipid extracts (TLE) were separated into polarity fractions using silica gel column chromatography. The apolar, ketone and polar fractions containing *n*-alkanes, alkenones, and glycerol dialkyl glycerol tetraethers (GDGTs) were eluted using *n*-hexane, DCM, and a 1:1 mixture of DCM and MeOH, respectively. After drying, the apolar and ketone fractions were dissolved in 50 µl *n*-hexane. The polar fractions were dissolved in *n*-hexane:isopropanol (95:5, v:v) and filtered through a 0.45 µm Polytetrafluoroethylene (PTFE) filter prior to analysis.

Alkenone and *n*-alkane measurements were carried out on an Agilent 7890 series II gas chromatograph equipped with an on-column injector and a Flame Ionization Detector (GC-FID) at the Institute of Geology and Mineralogy, University of Cologne. A fused silica capillary column (DB-5MS; 50 m x 0.2 mm, film thickness: 0.33 µm) was used with He as carrier gas. The samples were injected at 70°C, and the consecutive GC oven temperature was raised to 150°C at a rate of 20°C/min. By 150°C the temperature increase was reduced to 6°C/min to 320°C, which was held for 40 min. Both alkenones and *n*-alkanes were determined and quantified by authentic external standards.

Analytical precision for alkenone and *n*-alkane measurements was < 5% based on replicate standard analyses.

GDGTs were analyzed using ultra-high performance liquid chromatography (UHPLC; Agilent 1290 Infinity II) coupled to an Agilent 6460 Triple Quadrupole Atmospheric Pressure Chemical Ionization Mass Spectrometer (QQQ APCI MS) after the method from (Hopmans et al., 2016) at the Institute of Geology and Mineralogy, University of Cologne. Improved separation of 5- and 6-methyl branched GDGTs (brGDGTs) was augmented by using two coupled UHPLC silica columns (BEH HILIC columns, 2.1 x 150 mm, 1.7 µm; Waters™) connected with a guard column maintained at 30°C at a flowrate of 0.2 ml/min. Determination of specific GDGTs was accomplished by single ion monitoring and quantified using an internal C_{46} standard (Huguet et al., 2006), presuming a congruent response between the standard and measured GDGTs. Reproducibility of GDGT concentrations was < 9 %.

Concentrations of alkenones, *n*-alkanes, brGDGTs and crenarchaeol were converted to Mass Accumulation Rates (MAR) to ensure their independency of other sedimentary components. MARs were calculated as follows:

$$MAR_{bio}\left[\frac{\mu g}{ka\ \ cm^2}\right] = DBD\ \left[\frac{g}{cm^3}\right] \times SR\ \left[\frac{cm}{ka}\right] \times C_{bio}\left[\frac{\mu g}{g}\right]$$

where DBD is Dry Bulk Density calculated from sample volume and its dry weight, SR is the sedimentation rate and C_{bio} correspond to concentrations of alkenones, *n*-alkanes, brGDGTs or crenarchaeol (**Supplementary Material Figure S2**).

The Branched and Isoprenoid Tetraether (BIT) index was calculated as defined by (Hopmans et al., 2004):

$$\mathrm{BIT}_{index} = \frac{[I + II + III]}{[I + II + III] + [IV]}$$

where the roman numerals I, II and III refer to the non-isoprenoidal brGDGTs originating from terrestrial anaerobic soil bacteria. The group IV refers to the characteristic isoprenoidal GDGT "crenarchaeol" of aquatic Thaumarchaeota (formerly named Crenarchaeota) from marine environments. The BIT index is used to assess the relative fluvial input of terrestrial organic matter to marine environments and ranges from 0 (exclusively marine organic matter) and 1 (exclusively terrestrial organic matter) (Hopmans et al., 2004; Huguet et al., 2007).

Alkenones in marine sediments originate from haptophyte algae (i.e., coccolithophorides, dominated by *Emiliania huxleyi*) and high flux rates may therefore reflect higher surface oceanic productivity (Prahl et al., 1993; Rostek et al., 1997; Kirst et al., 1999; Herbert, 2014; Jaeschke et al., 2017). Long-chain *n*-alkanes are components of leaf-waxes from vascular plants and can be used as tracer for terrestrial input of organic matter to marine sediments (Freeman and Pancost, 2014; Jaeschke et al., 2017). Yet, *n*-alkanes may also source from bacterial degradation or matured contaminants. However, the calculated carbon preference index (CPI) from Core M125-35-3 is at average 3.2 (not shown), thus relatively high and comparable to modern soils, pointing to a predominance of well preserved terrestrial *n*-alkanes (Freeman and Pancost, 2014). GDGTs are membrane lipids synthesized by both aquatic archaea and terrestrial bacteria. We present MARs of crenarchaeol, a unique isoprenoidal GDGT, which is assumed to be specific to nitrifying marine mesophilic Thaumarchaeota, which are the most abundant single group of prokaryotes in the oceans, thus reflecting secondary production in the upper ocean (Karner et al., 2001; Sinninghe Damsté et al., 2002b; Sinninghe Damsté et al., 2002a). Mass accumulation rates of crenarchaeol are assigned to reflect secondary production by nitrifying Thaumarchaeota in the upper ocean. Further, we focus on accumulation rates of brGDGTs, which were attributed to terrestrial soil bacteria (Schouten et al., 2000; Weijers et al., 2006) and indicate changes in surface erosion and discharge towards our core location.

Bulk Sediment Elemental Analysis

X-Ray Fluorescence (XRF) analysis was performed on an ITRAX XRF Core Scanner (Cox Analytical Systems, Sweden) at the Institute of Geology and Mineralogy, University of Cologne. The freeze dried and homogenized aliquots of Core M125-35-3 were pressed into sample cups and covered with Ultralene® foil. The samples were placed into the core scanner in series enabling continuous measurement sequences. The XRF Scanner was equipped with a chromium (Cr) X-ray tube set to a voltage of 30 kV and a current of 55 mA. All 89 measurements were carried out at 1 mm resolution along the sample cup surface and a counting time of 60 s per sample. The multiple measurements per sample were averaged to determine most representative elemental quantities. The measured XRF spectra were quantified by external in-house standard measurements. Samples of Core M125-35-3 were quantified by using a set of 30 in-house standards from DSDP Site 511. For each element presented in this study, the standard calibration curves reveal a strong correlation ($r^2 > 0.8$).

XRF-derived geochemical data from Core M125-35-3 were grouped into elements which were associated with terrigenous run-off (i.e. Al, Si, K, Fe, Ti) and Ca, reflecting marine biogenic carbonate. In addition, we utilize ln(K/Al) and ln(Al/Si) ratios, which have been used to infer changes in continental moisture availability favoring chemical weathering in monsoonal dominated realms (Chiessi et al., 2010; Govin et al., 2012; Clift et al., 2014; Croudace and Rothwell, 2015; Bahr et al., 2021). Here, ln(K/Al) represents a measure of the intensification of chemical weathering as K is indicative for minerals (i.e. illite, potassium feldspar) which are predominant in dry regions with increased rates of mechanical over chemical weathering (Yarincik et al., 2000; Zabel et al., 2001; Burnett et al., 2011). Al is associated in products of intensive chemical weathering, being especially enriched in kaolinite, which is characteristic for tropical humid conditions (Bonatti and Gartner, 1973; Govin et al., 2012). Modern clay mineral compositions along the eastern and southeastern South American continental shelf clearly reflect the weathering regime of the hinterland as kaolinite is

predominant in the southeast and illite increase northward as more arid conditions prevail in ESA (Tintelnot, 1995). Thus, downcore ln(K/Al) of Core M125-35-2 is a pertinent proxy reflecting changes in the clay mineral composition which is strongly dependent on hinterland chemical weathering intensity and hence, moisture availability (Bahr et al., 2021). As related to past hydroclimate, low (high) ln(K/Al) reflect wetter (drier) conditions within the catchment area. We further compare the ln(K/Al) record with the ln(Al/Si) ratio, which has previously been used as proxy for chemical weathering intensity in South America (Chiessi et al., 2010). Decreased ln (Al/Si) are due to increased fluvial input of fine-grained quartz-rich material caused by higher rates of physical erosion in line with less humid conditions, while higher Al indicates stronger chemical weathering during wetter conditions (Biscaye, 1965; Govin et al., 2012).

Foraminiferal Geochemistry

For stable carbon isotope ($\delta^{13}C$) analysis, all samples were wet-sieved over a 63 μm mesh and oven-dried at 40°C. To avoid size-related ontogenetic effects (Elderfield et al., 2002), foraminiferal tests were sampled from the 355-400 μm size fraction (Friedrich et al., 2012) of the dried sediment. At minimum 50-60 individual foraminiferal tests of the surface-dwelling foraminifera *Globigerinoides ruber* (pink variety) (Chiessi et al., 2007) were handpicked under a stereo microscope. Subsequently, foraminiferal tests were gently crushed between two glass plates and residual detrital sediments from the exposed test chambers was removed. The crushed foraminiferal tests were rinsed three times with ultrapure methanol and ultrasonicated between each rinsing step. Stable isotope measurements were carried out on a Thermo Fisher MAT 253plus mass spectrometer equipped with an automatic Kiel IV carbonate preparation system at the Institute for Earth Sciences, Heidelberg University (Germany). Isotope values were calibrated to an in-house carbonate standard (Solnhofen limestone) and are reported in per mil (‰) relative to Vienna Peedee belemnite [VPDB]. Analytic precision based on repeated measurements of the in-house standard is < 0.03 ‰ for $\delta^{13}C$.

Venancio et al. (2017) inferred from sediment-trap studies located off SE Brazil at 23.6°S, that *G. ruber* (p) is the best-suited planktonic foraminiferal species to reconstruct surface-ocean conditions in the western South Atlantic. The sediment trap study revealed no significant seasonal changes in the occurrence of *G. ruber* (p), thus likely reflecting annual mean conditions. The calcification depth of *G. ruber* (p) at this study site was determined by (Venancio et al., 2017) as the mixed layer between 30 and 40 m water depth, which is comparable to the estimated calcification depth of *G. ruber* in the Pacific Ocean (Rippert et al., 2016).

The $\delta^{13}C$ of planktonic foraminifera shells are used to reconstruct the carbon isotopic composition of dissolved inorganic carbon (DIC) in seawater during calcification. The ambient seawater $\delta^{13}C_{DIC}$ during foraminiferal calcification is influenced by numerous processes, which may be distinguished into biotic and non-biotic processes. With respect to biotic effects, $\delta^{13}C_{DIC}$ of seawater reflects local changes in the balance between photosynthesis (increasing in $\delta^{13}C$) and respiration (decreasing $\delta^{13}C$). In the surface ocean (i.e. habitat of *G. ruber* (p)*)*, however, photosynthesis dominates over respiration (Ravelo and Hillaire-Marcel, 2007). Thus, $\delta^{13}C_{plank}$ of Core M125-35-3 likely reflects the rate of photosynthesis and amount of exported ^{12}C enriched particulate organic matter from the reservoir. Non-biotic effects may comprise advection or upwelling of water masses with different $\delta^{13}C_{DIC}$ signatures. Since *G. ruber* (p) occurs throughout the entire record of Core M125-35-3 and this species is associated to the oligotrophic waters carried by the Brazil Current one would not expect a substitution of different water-masses. Additionally, foraminiferal respiration and symbiont activity may bias $\delta^{13}C$ in foraminiferal tests. However, as we analyze a single species within a narrow size range, our record should be uniformly affected by these influences. Thus, next to other productivity-proxies shown in this study, $\delta^{13}C_{plank}$ may give supporting evidence in the interpretation of oceanic paleo-productivity.

Age Model

The initial age model of Core M125-35-3 was published in (Meier et al., 2021). For this study, we modified the initial model as we added one additional AMS ^{14}C age to improve the accuracy of the late deglacial shift from the Bølling-Allerød (B/A) interstadial to the Younger Dryas (YD) stadial (**Table 1**). The AMS ^{14}C dating was performed by BETA Analytics Limited in Miami (USA). All AMS ^{14}C ages (**Table 1**) were recalibrated with the most recent MARINE20 calibration curve (Heaton et al., 2020) and as recent findings on the marine radiocarbon reservoir effect off the Brazilian coast were published by Alves et al. (2021), we considered a $\Delta R = -84 \pm 125$. As done in (Meier et al., 2021) we used the CRAN R package Bacon (version 2.5.7) (Blaauw and Christen, 2011) to constrain the chronostratigraphy of Core M125-35-3. AMS ^{14}C were calibrated within the Bacon software using a student-t-distribution (Christen and Pérez, 2009) The improved age model covers the interval from ~19.3 ka to the late Holocene around ~4.0 ka comprising the last deglaciation, which we define as the period between the Last Glacial Maximum (LGM) and the beginning of the Holocene (H) including HS1, the B/A, and the YD. Sedimentation increase from ~10 cm/kyr during the latest LGM to maximum values of ~18.0 cm/kyr during the early deglaciation along HS1. After ~14.2 ka, sedimentation rates decrease rapidly to minimum values of ~4.0 cm/kyr. From the onset of the Holocene at ~11.7 ka, sedimentation rates slightly increase to 8 cm/kyr at the youngest part of the record at 4.0 ka (**Figure S1** in **Supplementary Material**).

RESULTS

The elemental ratios ($\Sigma_{Fe, Al, Ti, K}$)/Ca and biomarker proxies (MARs of brGDGTs and the BIT index) which are typically associated with continental runoff, reveal a steady deceasing trend during HS1 (**Figures 3H–J**). In contrast, mass accumulation rates of *n*-alkanes show increasing values and higher variability during HS1 (**Figure 3G**). Plant input, as inferred from long-chain *n*-alkanes, show an increased input of

TABLE 1 | Calibrated AMS ^{14}C ages measured on the planktonic foraminifera *Globigerinoides ruber* (pink) using the software Calib (version 8.2) and the MARINE20 calibration curve with ΔR = -81 ± 124.

Depth (cm)	Lab code	^{14}C age (yr BP)	Error of ^{14}C ages (yr)	2σ calibrated age range (cal yr BP)	Calibrated Median Age Probability (cal yr BP)	Remarks
25.5	BE-7261.1.1	3743	± 42	3261 - 3971	3610	
44.5	Beta-530016	6800	± 30	6878 - 7468	7189	
60.5	BE-7267.1.1	9414	± 43	9760 - 10535	10178	
67.5	Beta-606506	11200	± 30	12313 - 12927	12633	This study
75.5	Beta-530017	12890	± 40	14161 - 15104	14660	
90.5	BE-7268.1.1	12781	± 52	14027 - 14968	14492	
120.5	BE-7269.1.1	13516	± 54	15153 - 15970	15552	
150.5	BE-72701.1	14254	± 59	16118 - 16930	16518	
159.5	Beta530018	15780	± 40	18019 - 18685	18357	

If not specified, data are from Meier et al. (2021).

plant-derived organic matter at Core M125-35-3 from the end of LGM towards the late HS1 with maximum values around 3200 ng cm^{-2} ka^{-1} at ~15.0 ka. Remarkably, all biomarker-based proxies of Core M125-35-3 (alkenones, *n*-alkanes, brGDGTs and crenarchaeol) reveal a rapid decrease in coincidence with the onset of the B/A at ~14.6 ka (**Figures 3D, E, G, H**). Subsequently, the BIT index, *n*-alkane MARs and ($\Sigma_{Fe, Al, Ti, K}$)/Ca remain stable at very low values throughout the rest of the study interval. MARs of brGDGTs, crenarchaeol and alkenones of Core M125-35-3 mimic this pattern, but show an increase after ~7.0 ka during the mid-Holocene, which is of much higher amplitude in crenarchaeol and alkenone MARs (**Figures 3D, E, H**).

$\delta^{13}C_{plank}$ remains relatively constant during HS1 and increases steadily by ~0.5 ‰ during the Holocene (**Figure 3C**). In contrast, alkenone and crenarchaeol MARs reveal distinctly higher oceanic productivity during HS1, approach minimum values during the early Holocene, and show a subsequent continuous increase that accelerates after ~7 ka.

Both, ln(Al/Si) and ln(K/Al) ratios indicate slightly wetter conditions across the catchment of the Paraíba do Sul during HS1 compared to the LGM (**Figures 3A, B**). Drier conditions prevail during the B/A followed by a slight increase in moisture availability across the Paraíba do Sul catchment during the YD stadial. During the Holocene, a long-term decrease of ln(K/Al) and an increase of ln(Al/Si) reveals successively wetter conditions. Overall, precipitation variability in the Paraíba do Sul catchment during the deglacial is comparable or even slightly smaller than that of the Holocene (**Figures 3A, B**).

DISCUSSION

Effects of Enhanced Deglacial and Holocene Fluvial Run-Off on the Marine Environment

On longer time scales, spanning the entire record, our results reveal that a number of proxies from Core M125-35-3, which are commonly used to reconstruct terrestrial related environmental changes reveal a distinct correlation with the deglacial sea level rise defining the extension of the exposed continental shelf (**Figures 1**, **3**). Namely, elemental ratios typically associated with continental runoff ($\Sigma_{Fe, Al, Ti, K}$)/Ca, MARs of brGDGTs and the BIT index are clearly anti-correlated with the deglacial rising sea level (**Figures 3H–K**) and reveal a steady decreasing trend from the LGM towards the B/A. Yet an exception are *n*-alkane MARs, which display increasing values during HS1 prior to their rapid decrease at the onset of the B/A (**Figure 3G**). A secondary source of *n*-alkanes, which may bias the *n*-alkane MARs can be excluded, as the calculated carbon preference index (CPI) from Core M125-35-3 is at average 3.2 (not shown), thus relatively high and comparable to modern soils, pointing to a predominance of well preserved terrestrial *n*-alkanes (Huang et al., 1996; Freeman and Colarusso, 2001; Freeman and Pancost, 2014). The HS1 pattern of *n*-alkane concentrations corresponds well to the evolution of speleothem $\delta^{13}C$ values of Botuverá Cave located in SE Brazil (27°S) (Cruz et al., 2005) (**Figures 3F, G**). Amongst others, speleothem derived $\delta^{13}C$ provides information of biogenic activity above the cave and/or changes in the relative proportion of C_3 (trees and shrubs) to C_4 (drought-adapted grasses) vegetation, with C_3-plants having a lighter $\delta^{13}C$ signature than C_4 plants (Fleitmann et al., 2008; Novello et al., 2019). Here, we ascribe increasing *n*-alkane concentrations occurring parallel to decreasing $\delta^{13}C$ values of Botuverá Cave to the expansion of C_3-dominated Atlantic rainforest (tropical evergreen forest) onto the exposed shelf and the presence of subtropical gallery forests along the Paraíba do Sul during HS1 both substituting the tropical seasonal forest, savanna and grassland-dominated flora prevalent during the LGM. This is in line with late Pleistocene pollen-based reconstructions from Southern and SE Brazil suggesting an expansion of Atlantic rainforests and gallery forests after 17.0 ka (Behling, 1997; Behling, 2002; Gu et al., 2018) and somewhat later starting at 15 ka in SESA (Gu et al., 2017; Gu et al., 2018). The numerical modelling experiments from Maksic et al. (2022) further corroborate the described changes in biomes. Simultaneously, soil run-off decreased as observed from brGDGTs mass accumulation rates during HS1, which may indicate suppressed top-soil erosion induced by forest expansion (**Figure 3H**). The successive decrease in organic matter of terrestrial origin and especially the sudden decrease in both *n*-alkanes and brGDGTs during the B/A and Holocene point at a significantly reduced input of terrigenous organic matter to the upper slope likely amplified by other mechanisms (see *Discussion* below).

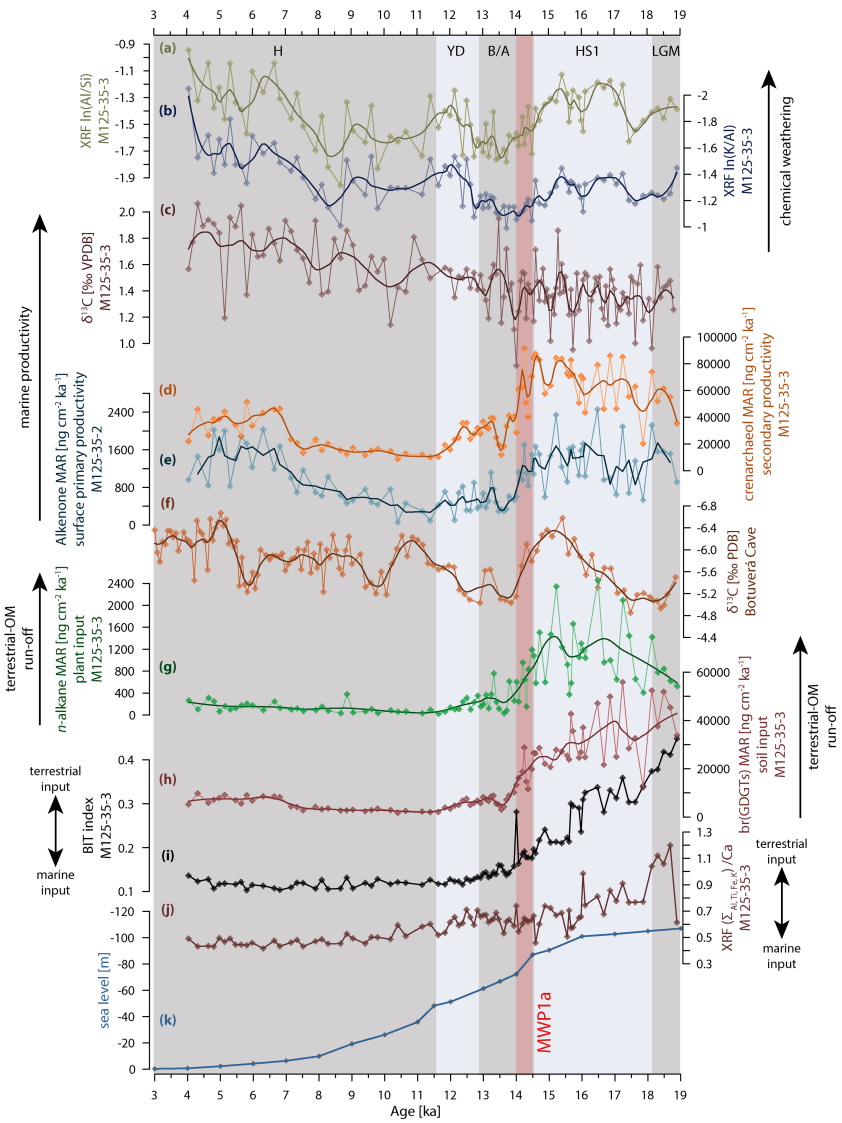

FIGURE 3 | Time series of lipid biomarker **(D, E, G, H, I)**, bulk sediment elemental composition **(A, B, J)** and foraminiferal geochemistry **(C)** data of Core M125-35-3 (this study) compared to a deglacial sea level **(K)** sea level reconstruction (Austermann et al., 2013) and terrestrial speleothem $\delta^{13}C$ **(F)** of Botuverá Cave (Cruz et al., 2005). Thick lines in panels a-h indicate 3-point running average. Bulk sediment elemental composition from Core M125-35-3: **(A)** ln(Al/Si), **(B)** ln(K/Al), j) ($\Sigma_{Fe, Al, Ti, K}$)/Ca. Lipid biomarker of Core M125-35-3): **(D)** Mass accumulation rate (MAR) of crenarchaeol, e) alkenone MAR, g) *n*-alkane MAR, **(H)** brGDGTs MAR, i) BIT index. **(C)** Stable carbon isotopes ($\delta^{13}C$) composition of *Globigerinoides ruber* (p). Arrows indicate direction of increases. Red shaded area marks the timing of Meltwater Pulse 1a (Brendryen et al., 2020). LGM, Last Glacial Maximum; HS1, Heinrich Stadial 1; B/A, Bølling-Allerød interstadial; YD, Younger Dryas; H, Holocene; MWP1a, Meltwater Pulse 1a.

Terrestrial input into oligotrophic waters carried by the Brazil Current alongshore southeastern Brazil would provide an important nutrient source for oceanic biota. In fact, high marine productivity at Core M125-35-3 during HS1, reflected by the increase in alkenone and crenarchaeol accumulation rates (**Figures 3D, E**) aligns with elevated accumulation rates of terrigenous elements (Fe, Al, Ti, K) (**Figure S3** in **Supplementary Material**), *n*-alkanes and brGDGTs (**Figures 3G, H**) pointing at high siliciclastic and organic matter input of terrestrial origin. Notably, the accumulation rates of Fe, Al, Ti, and K as well as Ca are high during HS1, which agrees with the presumption that enhanced marine productivity during higher terrestrial run-off increases deposition of carbonate and the relative content of Ca in the sediment (Govin et al., 2012). Thus, it is consistent to assume that a slightly invigorated continental hydrological cycle and particularly a marked low sea level enhanced nutrient and organic matter flux into the western tropical South Atlantic during HS1, boosting oceanic productivity. This proposed link between river run-off and marine productivity further fits to the suggestion that cold-water coral mounds in the vicinity of Core M125-35-3 flourished during times of enhanced organic-matter input from the continent due to enhanced nutrient and organic-matter availability (Bahr et al., 2020). To summarize,

we infer that terrestrial siliciclastic sediment and organic-matter flux to the upper slope off the Paraíba do Sul was maximal during HS1 and subsequently declined during the late deglacial and Holocene, largely owing to the rising eustatic sea level and ensuing coastline retreat.

Against the above discussed scenario, one might argue that $\delta^{13}C_{plank}$ values remain constantly low during HS1, instead of the expected more enriched values in response to high surface productivity. However, the isotopic fractionation of DIC due to enhanced marine productivity during HS1 may have been compensated by the enhanced input of terrestrial organic matter which is considerably depleted in ^{13}C. The $\delta^{13}C$ in the western subtropical South Atlantic must be considered an open system, where the reservoir and fixation of light ^{12}C by oceanic productivity is constantly compensated by run-off of terrestrial organic matter resulting in no notable fractionation in our $\delta^{13}C_{plank}$ record during HS1.

Interestingly, the rapid decrease in MARs of crenarchaeol, alkenones, *n*-alkanes and brGDGTs at ~14.6 ka at the onset of the B/A coincides with meltwater pulse 1a (Weaver et al., 2003; Brendryen et al., 2020), a phase of rapid sea level rise in which sea level rose by ~20 m within ~500 years (Liu et al., 2016) (**Figures 3D, E, G, H**). We note, that the rapid decrease in *n*-alkanes and brGDGTs might be intensified by a shift to slightly dryer conditions during the B/A onset as reflected by our ln(K/Al) and ln(Al/Si) records leading to decreased terrestrial run-off (**Figures 3A, B**). However, as existing pollen-based vegetation records of the Atlantic rainforest do not reveal a marked decrease or retreat (Gu et al., 2017; Gu et al., 2018), we infer that changes in the hydroclimate were rather small. Thus, we argue that meltwater pulse 1a marks a threshold, facilitated by the broad shelf off SE Brazil, when transgression suddenly flooded a wide area (**Figure 1**), which functions as a sediment trap during interglacial high sea level stands. Indeed, a similar situation was previously described for southern Brazil and Uruguay (Chiessi et al., 2008; Lantzsch et al., 2014). After flooding the shelf, the influx of terrestrial (organic) matter to the continental slope was substantially reduced and became rather insensitive to continental climatic variability compared to the period before the B/A that is characterized by high sediment input to the slope. Yet, during the Holocene, high $\delta^{13}C_{plank}$ as well as high accumulation rates of alkenone and crenarchaeol synthesizing Coccolithophorides and Thaumarchaeota, respectively (**Figures 3C–E**), point at increased oceanic productivity. Further, the BIT index remains low during the Holocene, although a slight increase of terrestrial-derived brGDGTs is observed (**Figures 3H, I**). This slight enhanced input of brGDGTs is apparently compensated by the increase of crenarchaeol in Core M125-35-3 due to higher marine productivity, which in sum leads to a low BIT index (**Figures 3D, H, I**). The dominance of marine organic matter during the Holocene is in line with the more distant shore line, especially after MWP 1a flooded the shelf (**Figure 3**), when terrestrial sediment and organic matter input to the upper slope were significantly reduced. However, as increasing ln(Al/Si) and decreasing ln(K/Al) ratios indicate successively wetter conditions after 8.5 ka, we argue that increased oceanic productivity during the Holocene was caused by increased terrestrial runoff fostered by successively wetter conditions across the Paraíba do Sul catchment eventually providing nutrients to the sub(tropical) South Atlantic. Nonetheless, increased river runoff in line with higher precipitation during the Holocene was less efficient in affecting the oceanic nutrient inventory than the sea-level fluctuations during the deglacial. This is also supported by the lower Holocene MARs of alkenones and crenarchaeol when compared to HS1. In addition, the isotopic fractionation displayed by $\delta^{13}C_{plank}$ may point to limited influx of ^{13}C-depleted terrestrial organic matter and diminished deposition in terrestrial derived sediments.

Deglacial and Holocene SAMS/SACZ Precipitation Variability Across South America

Previous studies have emphasized the role of an intensification and/or expansion of the SACZ for providing enhanced moisture for ESA and SESA during HS1 (Stríkis et al., 2015; Novello et al., 2017; Stríkis et al., 2018; Venancio et al., 2020). As the Paraíba do Sul catchment is within the core region of the SACZ, our record from Core M125-35-3 is, when combined with available paleo-hydrological records from its northern and southern boundaries, ideally suited to track both the strength and area of the SACZ. For this purpose, we compare our results with published trace metal data from speleothems from Botuverá Cave (27°S), which is located just south of the modern domain of the SACZ (Cruz et al., 2007) and $\delta^{18}O$ records of Lapa Sem Fim (16.1°S) and Paixão Caves (12.6°S) located to the north of the SACZ (**Figures 1**, **4C, D, I, J**).

Based on the ln(K/Al) and ln(Al/Si) data from Core M125-35-3 (**Figures 4A, B**), we suggest that precipitation intensity in the core domain of the SACZ (at least over the Paraíba do Sul catchment) did not vary markedly over the deglaciation, with slightly more precipitation during HS1 and the YD compared to the drier B/A. Indeed, neither of these intervals stick out as a climatic extreme in Core M125-35-3.

Trace metal data from Botuverá Cave (Sr/Ca and Mg/Ca) (Cruz et al., 2007) indicate an overall decreasing trend during HS1 pointing to progressively drier conditions (**Figures 4C, D**). Today, Botuverá Cave receives precipitation all year round with no pronounced dry season (during austral summer moisture derives from the SACZ/SAMS, during austral winter moisture is related to extra tropical cyclones (Gan and Rao, 1991; Vera et al., 2002). During HS1, however, a greater seasonal contrast in rainfall probably characterized the region, with a dry season during austral winter and wet austral summer season induced by the SAMS/SACZ. This is supported by palynological studies from southern and southeastern Brazil indicating the dominance of *Poaceae* reflecting rather cold and dry conditions, while modern-like *Araucaria* forests, which are intolerant to long dry seasons, were absent (Behling, 2002; Gu et al., 2017; Gu et al., 2020). A greater seasonal contrast is also supported by low $\delta^{18}O$ values in Botuverá Cave speleothems that point at the Amazon basin as the dominant moisture source

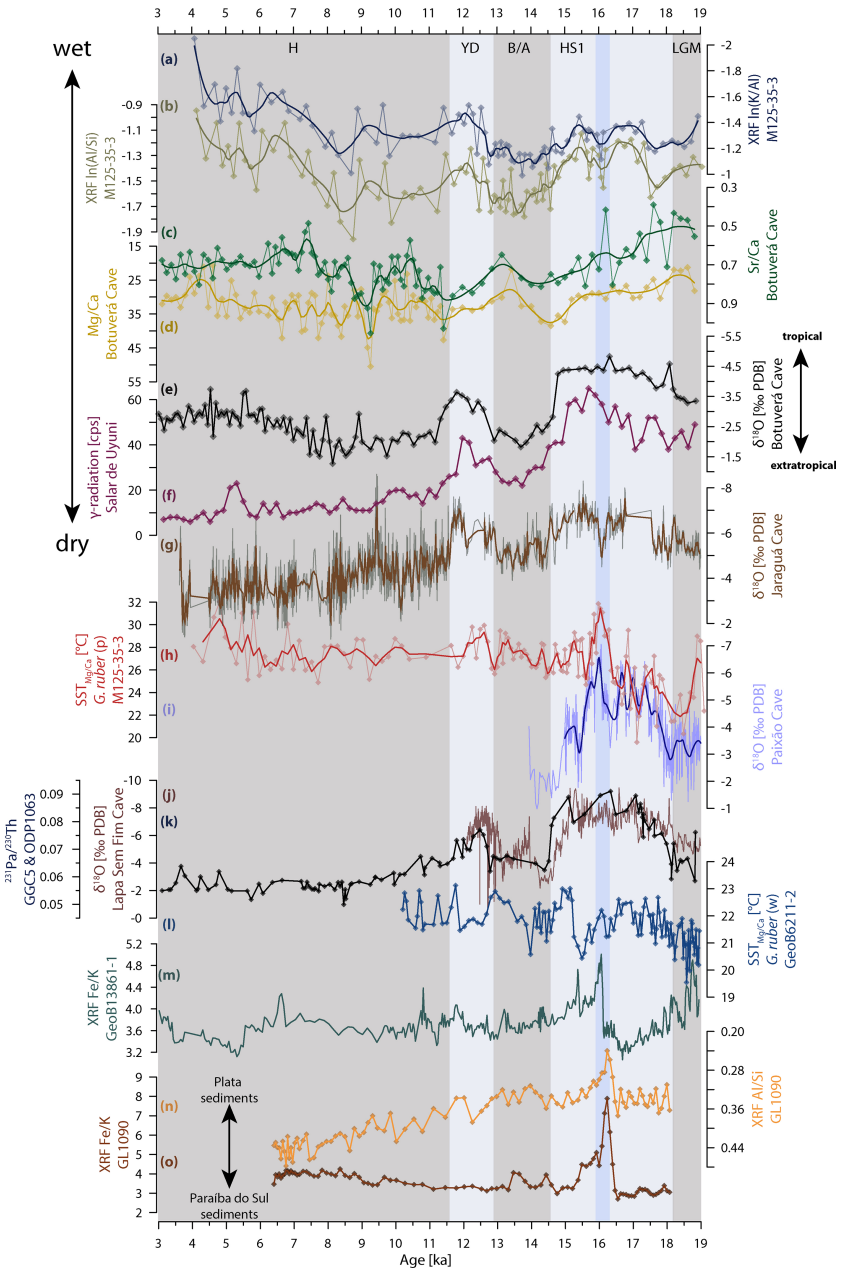

FIGURE 4 | Compilation of paleo precipitation records from South America together with sea-surface temperature (SST) reconstructions from the sub(tropical) South Atlantic. The blue shaded area marks the timing of the atmospheric adjustment to a negative like SALLJ/SACZ dipole pattern across South America at ~16.0 ka as explained in the main text (SALLJ: South American Low Level Jet, SACZ: South Atlantic Convergence Zone). **(A)** ln(Al/Si)) and **(B)** ln(K/Al) of Core M125-35-3 (this study). **(C)** Speleothem-based Sr/Ca, **(D)** Mg/Ca and **(E)** $\delta^{18}O$ of Botuverá Cave located in southeastern South America (Cruz et al., 2005, 2007). **(F)** γ-radiation based precipitation record from Salar de Uyuni located in the central Andes (Baker et al., 2001). **(G)** Speleothem-based $\delta^{18}O$ of Jaraguá Cave in central South America (Brazil) (Novello et al., 2017). **(H)** Mg/Ca-based SST reconstruction from Core M125-35-3 (Meier et al., 2021), **(I)** Paixão Cave speleothem based $\delta^{18}O$ ‰ records and **(J)** Lapa Sem Fim Cave speleothem based $\delta^{18}O$ compilation (Strikis et al., 2015, 2018) from eastern South America, **(K)** $^{231}Pa/^{230}Th$ compilation from Core GGC5 and ODP Site 1063 representing Atlantic Meridional Overturning Circulation strength (McManus et al., 2004; Böhm et al., 2015; Lippold et al., 2019), **(L)** $SST_{Mg/Ca}$ record of Core GeoB6211-2 (Chiessi et al., 2015) collected off southern Brazil, **(M)** XRF-derived Fe/K from Core GeoB13861-1 close to the La Plata River mouth (Warratz et al., 2017). **(N)** and **(O)** XRF derived ln(K/Al) and Fe/K from Core GL-1090 from the La Plata River mouth (Mathias et al., 2021). Thick lines in panels a-d and g-i indicate 3-point running average. LGM, Last Glacial Maximum; HS1, Heinrich Stadial 1; B/A, Bølling-Allerød interstadial; YD, Younger Dryas; H, Holocene; MWP1a, Meltwater Pulse 1a.

during HS1 (Bernal et al., 2016), which today fuels the SACZ. Hence, based on available data from Botuverá Cave, a reduction in winter-time precipitation can be inferred, while the SACZ-related precipitation appeared to have been relatively stable.

Intensification of SAMS/SACZ activity over ESA during HS1 was previously suggested by Stríkis et al. (2015) based on speleothem precipitation records from Lapa Sem Fim and Paixão Caves (**Figures 1**, **4I, J**). The positive precipitation anomalies in Lapa Sem Fim and Paixão Caves were related to so-called "Mega-SACZ-Events" that were presumed to be a consequence of enhanced convection of tropical-sourced moisture towards ESA and SESA (Stríkis et al., 2015). However, the new ln(K/Al) and ln(Al/Si) records of Core M125-35-3 do not support a strong intensification of the SACZ during HS1 (**Figures 3A, B**). The more frequent $\delta^{18}O$ minima in both cave records may be explained by northward expansions of the SACZ leading to increased precipitation above the cave sites. The core region of the SACZ, on the other hand, seems unaffected by potential northward expansions as the Paraíba do Sul catchment remains within the SACZ influence as inferred from ln(K/Al) and ln(Al/Si) of Core M125-35-3. An exception occurred around ~16 ka, when a minimum in $\delta^{18}O$ indicate the wettest phase in the Paixão record. Minimum $\delta^{18}O$ occurs synchronously with slightly dryer conditions across the Paraíba do Sul catchment area suggesting a northward displacement of the SACZ.

Interestingly, the Paixão Cave $\delta^{18}O$ record closely follows the Mg/Ca-based SST reconstruction of Core M125-35-3 (Meier et al., 2021) (**Figures 3H, I**). Further, the compiled $\delta^{18}O$ records of Lapa Sem Fim Cave (Stríkis et al., 2015; Stríkis et al., 2018) match remarkably well with the $^{231}Pa/^{230}Th$ compilation record of cores GGC5 and ODP Site 1063 from the North Atlantic (McManus et al., 2004; Böhm et al., 2015; Lippold et al., 2019), indicating a sluggish AMOC during HS1 (**Figures 3J, K**). These correlations may imply a connection between large-scale oceanographic changes in the western South Atlantic and precipitation pattern across ESA during HS1. Campos et al. (2019) showed that precipitation variability in ESA and SESA was driven by a mechanism independent of SAMS/SACZ activity. Campos et al. (2019) proposed that precipitation availability in ESA and to a lesser degree in SESA depended on atmospheric and oceanographic changes that resulted from the diminished interhemispheric heat transfer caused by a weakened AMOC. Based on model and proxy data, Campos et al. (2019) inferred that increased (decreased) moisture sourced from the warmer (colder) tropical South (North) Atlantic was transported with the SE (NE) trade winds during austral summer (winter). In fact, the good correlation of high SSTs at Core M125-35-3 and increased precipitation above Paixão Cave indicate that SSTs from the sub(tropical) South Atlantic played a crucial role in determining the amount of moisture advected by the SE winds towards ESA and SESA. High (low) SSTs in the sub(tropical) western South Atlantic probably contributed to warm and moist (cool and dry) air towards the continent. In contrast, the southerly located Botuverá Cave in SESA seems to be unaffected by this oceanic sub(tropical) moisture source as its precipitation record reveals continuously dryer conditions, especially during austral winter. It thus appears that during HS1 SE trade winds delivering oceanic-sourced moisture were primarily responsible for enhanced precipitation in tropical ESA (e.g., at Paixão and Lapa Sem Fim Caves) and to a lesser degree in the south where they contributed to the slightly wetter conditions across the Paraíba do Sul catchment. A gradual trend towards increasing precipitation in the northern portions of ESA may imply a relative increase in convective rainfall associated with a marked southward shift of the ITCZ during HS1. However, reconstructions of deglacial migrations of the ITCZ during northern hemispheric cooling suggest southward shifts of no more than 7° from its modern position (Arbuszewski et al., 2013; Schneider et al., 2014; Portilho-Ramos et al., 2017). A significant contribution of ITCZ rainfall to ESA is hence unlikely.

In addition, Chaves and Nobre (2004) showed that, based on observational data, positive SST anomalies in the western subtropical and tropical South Atlantic lead to a northward shift of the SACZ. This corroborates the interpretation that not a substantial intensification of the SACZ increased precipitation during HS1, but northward shifts/expansions of the SACZ additionally amplified precipitation in SESA as illustrated by the synchronous SST maximum at Core M125-35-3 and peak precipitation at the Paixão Cave record at ~16.0 ka (**Figures 4H, I**, **5**). Our findings lead us to recede from the previously suggested "Mega-SACZ-Event" and suggest that the slight increased precipitation in ESA and SESA during HS1 was primarily due to enhanced moisture advection from the tropical western South Atlantic. However, northward expansion or potential shifts of the SACZ might have additionally reinforced precipitation in ESA. Hence, our findings corroborate the mechanism proposed by Campos et al. (2019) for positive precipitation anomalies over tropical South America.

South American Low Level Jet Dynamics During the Deglaciation

While the deglacial hydroclimate variability in ESA and partially in SESA might be well explained by changes in trade wind intensity and SACZ dynamics, precipitation patterns across SSESA are strongly influenced by synoptic-scale climate features, that are usually insufficiently considered in paleoclimatic studies

The XRF-derived Fe/K record from Core GeoB13861-1 (38.0° S) (Warratz et al., 2017) collected off the La Plata River mouth (**Figures 1**, **4M**), as well as the Fe/K and Al/Si records from Core GL-1090 (24.92°S) (Mathias et al., 2021) retrieved off SE Brazil potentially show precipitation changes over SSESA, the southern part of the dipole. We updated the age model of Core GL-1090 applying the new MARINE20 calibration curve (Heaton et al., 2020) to enable a robust correlation with Core M125-35-3.

From the LGM towards ~16 ka, the Al/Si record of Core GL-1090 reveals relatively high values indicating smaller amounts of sediments from the La Plata River (**Figure 4N**) in SSESA. The Fe/K record of Core GeoB13861-1 displays decreasing values from the LGM to 16 ka, indicating a decreasing runoff of deeply

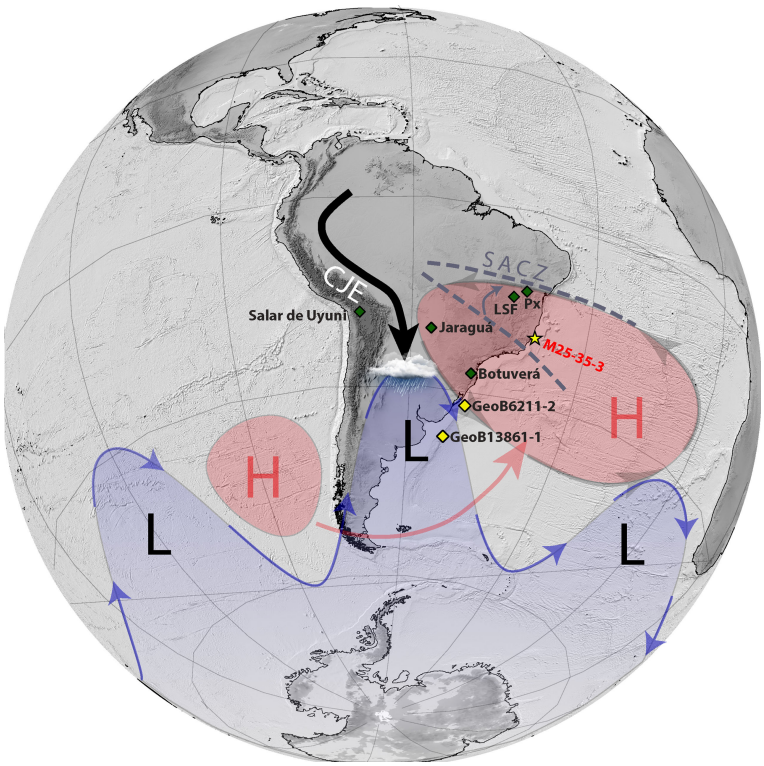

FIGURE 5 | Schematic illustration of atmospheric circulation patterns and rainfall anomalies in South America during Heinrich Stadial at ~16 ka. The blue shaded area marks the low-pressure system related to the steady eastward propagating Rossby wave train. High-pressure systems propagate northward as they pass the Andes (indicated by the red arrow). The quasi-stationary system that occurred at ~16 ka during HS1 foster a subtropical high-pressure system across South America (red area above South America). Substantial moisture transport *via* the Chaco Jet Event (CJE) configuration (black arrow) enhances rainfall in southern southeastern South America. Under this situation, the South Atlantic Convergence Zone (SACZ) was likely displaced northward relative to its modern position. Green and yellow diamonds indicate terrestrial and marine previously published precipitation records respectively. Px, Paixão Cave; LSF, Lapa Sem Fim Cave The yellow star marks Core M125-35-3 (this study).

weathered material from the Paraná catchment and the La Plata basin (**Figure 4M**). However, these values need to be interpreted with caution since decreased bottom current activity favors the deposition of fine grained clays of Al-rich illite and chlorite (which may contain significant amounts of Fe) from the circumantarctic area, potentially increasing Fe/K values during the late LGM and early HS1 (Warratz et al., 2017). However, the Fe/K record from Core GL-1090, collected ca. 10° to the north and ca. 1500 m shallower than GeoB13861-1, constantly displays low values from the LGM towards ~16.0 ka (**Figure 4O**) which is unlikely an effect of the northward dispersal of clays from the Southern Ocean [cf. **Figure 4** in (Warratz et al., 2017)]. Overall, we infer that hinterland runoff *via* the La Plata River and associated precipitation across the Paraná catchment in SSESA was relatively low between ca. 18 and 16 ka. As discussed above, ln(K/Al) and ln(Al/Si) ratios from Core M125-35-3 reveal slightly elevated precipitation during this interval (**Figures 4A, B**). Silva and Berbery (2006) observed a strong thermal front in the vicinity of southern Brazil during positive precipitation anomalies in SSESA. If this thermal front is not or only weakly established, precipitation in the SACZ region is enhanced. Indeed, SST from Core M125-35-3 are rather low and show an increasing trend from ca. 18 until 16 ka, comparable to the southerly located Mg/Ca-based SST record of Core GeoB6211-2 (32.5°S) collected off southern Brazil (Chiessi et al., 2015) (**Figure 4L**) pointing at a weak meridional SST gradient. Thus, we suggest that more moisture was transported towards the SACZ realm in SESA *via* the NCJE configuration. The dipole precipitation pattern was thus rather adjusted to a positive (increased) precipitation in SESA at the expense of dryer conditions in SSESA (**Figures 1**, **5**).

At ~16.0 ka a distinct change in the SACZ-SALLJ dipole configuration occurs, as displayed by the signal and spatial distribution of ensemble of precipitation records across South America presented in **Figure 4**. Noteworthy, the interval around 16 ka was associated to the most intense phase of Heinrich Event 1 (HE1) during HS1 and was characterized by the strongest thermal imbalance according to the interhemispheric seesaw (Meier et al., 2021). This pronounced phase of the interhemispheric thermal seesaw led to warming in the high-latitude southern South Atlantic, implying a markedly reduced equator to pole thermal gradient (Barker et al., 2009). These boundary conditions were also invoked to explain the vigorous warming in the western South Atlantic as observed in Mg/Ca-

based SSTs of Core M125-35-3 (**Figure 4H**) (Meier et al., 2021). During this interval at ~16.0 ka, the Jaraguá Cave speleothem record from central South America marks a distinct drying event (**Figures 1**, **3G**). Simultaneously, a distinct increase in Fe/K from Core GeoB13861-1 (Warratz et al., 2017) argues for marked wet events over the La Plata basin in SSESA (**Figure 3M**). Noteworthy, the Fe/K peak at ~16 ka at Core GeoB13861-1 coincides with a marked decrease in Al/Si of Core GL-1090 (**Figure 4N**), minimizing a potential imprint of allochthonous Al-enriched circumantarctic clays during times of relatively weak northward-flowing bottom currents (Warratz et al., 2017). We also infer that early diagenetic effects (e.g. by changing redox conditions) (Riedinger et al., 2005) are not the main cause for the Fe/K peak in Core GeoB13861-1 at ~ 16 ka as it coincides remarkably well with moist conditions over SSESA implied by the sudden decrease (increase) in Al/Si (Fe/K) of Core GL-1090 which during the deglacial was situated in a more proximal location relative to the La Plata River mouth due to the low sea level (Lantzsch et al., 2014; Mathias et al., 2021). At the same time, our ln(K/Al) and ln(Al/Si) record reveals a short intermittent dry period at 16.0 ka at the Paraíba do Sul catchment (**Figures 4A, B**). We note that ln(K/Al) and Si/Al from Core M125-35-3 as well as trace metal data from Botuverá Cave display rather moderate drying across the SACZ realm (**Figures 4A–D**). Missing tropical moisture export towards the SACZ domain in SESA *via* the NCJE would cause severely dry conditions which were, however, likely compensated by enhanced oceanic moisture flux in line with a vigorous warming in the western tropical South Atlantic (**Figure 4H**) at 16.0 ka. Thus, the precipitation pattern changed rapidly across South America at 16.0 ka towards a negative dipole configuration, where central South America (i.e. Jaraguá Cave) and SESA represented by Core M125-35-3 are characterized by drying and SSESA (i.e. the Paraná and Uruguay catchment) experienced distinct wet events. Notably, this precipitation dipole between SESA and SSESA coincided with the development of a distinct oceanographic front at around 16.0 ka in the western (sub)tropical South Atlantic as suggested by SST cooling at mid-latitude Core GeoB6211-2 (32.5°S) (Chiessi et al., 2015) parallel to pronounced warming at Core M125-35-3 (21.9°S) (Meier et al., 2021) (**Figures 4H, L**). As mentioned above, this thermal front is in line with increased precipitation in SSESA and drying in SESA, as observed by (Silva and Berbery, 2006). This pattern suggests that a strong and persistent CJE enhanced the flow of Amazon moisture towards the La Plata basin around 16.0 ka leading to anomalously high rainfall in SSESA. In this context, the concomitant dry phase at Jaraguá Cave is in line with the majority of Amazon moisture being transported southwards along the eastern margin of the Andes and to a lesser extend southeastward towards Jaraguá Cave and the Paraíba do Sul catchment area (**Figure 5**). Increased southward advection of Amazon moisture is also corroborated by a precipitation record from Salar de Uyuni on the Bolivian Altiplano in the central Andes showing increased rainfall throughout HS1 (**Figure 4F**) (Baker et al., 2001).

Although the negative precipitation dipole observed at ~16 ka fits to observational data such as the thermal front arising near SE Brazil (**Figures 4H, I**) (Silva and Berbery, 2006), there is still lack of a sufficient mechanism explaining the substantial reconfiguration of the lower atmospheric circulation and consecutive moisture transport across South America. Modern observations revealed that vast flooding and rainfall events may be strongly related to the behavior of Rossby wave propagation patterns. Extreme climate phases may be explained by high amplitude quasi-stationary Rossby waves resulting from a decreased atmospheric circulation caused by a reduction of the temperature difference between polar and mid-latitudes (Andreoli and Kayano, 2005; Coumou et al., 2014; Coumou et al., 2015; Coelho et al., 2016; Mann et al., 2017; Wolf et al., 2018). It is well documented that moisture flux by the SALLJ is largely dependent on the dynamics of synoptic-scale Rossby wave propagation (e.g. Salio et al., 2002; Carvalho et al., 2004; Liebmann et al., 2004; Marengo et al., 2004). We therefore suggest that around 16.0 ka, a time of maximum warming of the southern hemisphere due to the interhemispheric seesaw (Broecker, 1998; Stocker, 1998; Pedro et al., 2011; Barker and Diz, 2014; Meier et al., 2021), the overall decreased thermal gradient across the Southern Hemisphere led to a slowdown of the atmospheric circulation. Thus, the Rossby wave propagation became more stationary, leading to extreme and sustained climatic conditions in SSESA and SESA. The pattern suggests, that a strong subtropical high developed, which spread far across SESA, forcing the SALLJ to a NCJE-like configuration with an exit region above subtropical South America. Consequently, subsiding airmasses associated with a strong and stable subtropical high inhibited cloud cover leading to persistent radiative forcing, which likely fostered anomalously high SSTs as observed in Core M125-35-3 at 16 ka. This atmospheric and oceanic configuration in turn, led to vast increases in precipitation across SSESA. This pattern might be indirectly enhanced by a significantly southward shifted ITCZ at 16 ka. Climate models reveal a similar precipitation pattern across South America after significant weakening of the Southern Hemisphere Hadley cell affecting the subtropical and mid-latitude jets (**Figure 1** in Lee et al., 2011; Ceppi et al., 2013). Contrary, during the early and late phases of HS1, the atmospheric circulation and Rossby wave propagation was enhanced, leading to less pronounced and ephemeral extreme conditions similar to modern-like conditions. The dipole reconfiguration at 16 ka hence marks an anomalously persistent negative dipole mode lasting at least ~500 yrs (cf. blue shading in **Figure 4**). As discussed in Section 2, the occurrence of the negative dipole configuration such as at ~16 ka resembles hydroclimatic extremes of decadal- to interdecadal scales occurring under present-day conditions. However, modern trends and future projections of precipitation suggest an increase in the occurrence of the negative dipole pattern under quasi-stationary Rossby waves with hazardously increased rainfall across subtropical South America in SSESA due to global warming (Gonzalez et al., 2013; Junquas et al., 2013; Vera and Díaz, 2015; Saurral et al., 2017; Masson-Delmotte et al., 2021). It is astonishing that a similar climatic configuration could occur under considerably different boundary conditions. We hypothesize that both the future and the SACZ/SALLJ dipole evolution at ~16 ka respond to a common pattern, i.e., a reduced

hemispheric equator to pole thermal gradient as it is typical for both global warming scenarios (Masson-Delmotte et al., 2021) and HS1 (Barker et al., 2009).

Evolution of SAMS Dynamics After HS1

After HS1 (i.e., the late deglacial), ln(Al/Si) and ln(K/Al) of Core M125-35-3 suggest drier conditions during the B/A interstadial pointing to a weaker SAMS/SACZ which lasted until the beginning of the YD, when precipitation increased towards the onset of the Holocene (**Figures 4A, B**). This late deglacial pattern is consistent with the precipitation record from Jaraguá Cave (Novello et al., 2017) from the central domain of the SAMS/SACZ in central South America (Brazil) (**Figure 4G**). The strong late deglacial coupling of precipitation in the Paraíba do Sul catchment and Jaraguá Cave indicates that rainfall associated with the SAMS/SACZ intensity similarly determined precipitation in SESA and above Jaraguá Cave. If oceanic moisture would have dominated precipitation across the Paraíba do Sul catchment, one would a expect no clear correlation with the Jaraguá Cave speleothem record, located in central South America, distant from the coast (**Figure 5**). Indeed, SST cooling after 16 ka at the site of Core M125-35-3 implies less moisture export towards South America provided by evaporation over the sub(tropical) South Atlantic. Hence, we infer that during the late deglacial after HS1, oceanic moisture sourced from the (sub)tropical South Atlantic did not substantially contribute to moisture budget across SESA and a more modern-like precipitation pattern was established. Further, during the late deglacial the Fe/K and Al/Si of cores GeoB13861-1 and GL-1090 do not show any marked abrupt shift in precipitation across SSESA (**Figures 4M–O**). Thus, we assume, that late deglacial precipitation pattern associated with SACZ/SAMS variability was stabilized by the configuration of perpetually propagating non-stationary Rossby waves inhibiting sustained phases of extreme rainfall in SSESA such as during ~16 ka.

Drier conditions above the Paraíba do Sul catchment (**Figures 4A, B**) during the B/A can be assigned to the stabilization of temperatures in South America in coincidence with the Antarctic Cold Reversal indicating overall cooler and likely dryer conditions at the southern margins of the SAMS (Blunier et al., 1997; Chiessi et al., 2015; Pedro et al., 2016). Similarly to HS1, during the YD our records reflect a slight increase in SAMS/SACZ activity as recorded in Jaraguá Cave. This precipitation increase was likely related to warming of the Southern Hemisphere and enhanced moisture influx into South America due to Northern Hemisphere cooling leading to a southward shift of the ITCZ (Cruz et al., 2006; Novello et al., 2017). This is in contrast to the HS1, where the (sub)tropical western South Atlantic was involved as an important moisture source. SSTs of Core M125-35-3 indeed show a parallel warming trend during the YD, however, we assume that the quantity of oceanic-sourced moisture feeding SESA was greatly reduced because warming of the western tropical South Atlantic was much weaker compared to HS1.

From the mid Holocene (~8.5 ka) to the top of Core M125-35-3 our ln(K/Al) and ln(Al/Si) records reveal an increase in precipitation across the Paraíba do Sul catchment (**Figures 4A, B**). Simultaneously, the SST record from Core M125-35-3 shows an increase in temperatures towards ~30°C, which is somewhat lower as the SST peak at 16 ka (**Figure 4H**). At the same time, $\delta^{18}O$ from Jaraguá Cave shows decreased rainfall across central South America (**Figure 4G**). Supported by a slight decrease in the $\delta^{18}O$ Botuverá Cave record (**Figure 4E**), which shows an increased portion of oceanic moisture, we infer that during the mid- and late Holocene precipitation across SESA was enhanced by increased moisture flux from the sub(tropical) South Atlantic in line with higher SSTs.

CONCLUSIONS

Our deglacial multiproxy dataset of Core M125-35-3 reveals a strong impact of riverine run-off on marine biota in the western tropical South Atlantic and discloses new insights in the dynamics of the SAMS/SACZ. First, our data show that enhanced terrigenous nutrient and organic matter input fueled marine productivity in the realm of Core M125-35-3 during HS1, a consequence of low sea level and slightly enhanced continental precipitation. Second, vigorous warming of the (sub)tropical South Atlantic and substantial alteration of the atmospheric circulation during HS1 enhanced oceanic moisture flux towards eastern South America. Consequently, our findings imply that SAMS variability in SESA cannot be explained by changes in the intensity and geographic extent of the SACZ alone. Last, we demonstrate that reconstructions of rainfall patterns across SESA and SSESA need to consider the dynamics of Rossby wave trains and their influence on the SALLJ dynamics. Interestingly, numerical models imply that extreme climate conditions, as reflected by the persistent negative SALLJ/SACZ dipole pattern around ~16 ka during HS1, will likely recur under decisively different boundary conditions in the future as a consequence of global warming.

DATA AVAILABILITY STATEMENT

The datasets presented in this study can be found in online repositories. The names of the repository/repositories and accession number(s) can be found below: https://doi.pangaea.de/10.1594/PANGAEA.942656.

AUTHOR CONTRIBUTIONS

KM designed and conceptualized the study, took the lead in writing the manuscript, realized visualizations and conducted analytical work. AJ and JR conducted analytical work, aided in interpreting the results and worked on the manuscript. CC and OF contributed to the interpretation of the results and provided critical feedback and helped shape the manuscript. ALA contributed resources and contributed manuscript writing. VW conducted analytical work. AB contributed to the design of the study and implementation of

the research and contributed to the analysis interpretation of the results and writing of the manuscript. All authors contributed to the article and approved the submitted version.

FUNDING

AB acknowledges funding by the German Research Foundation (DFG; projects HO 5927/1-1 and BA 3809/14-1). AJ acknowledges financial support from DFG (grant 268236062 – SFB1211). CMC acknowledges financial support from FAPESP (grants 2018/15123-4 and 2019/24349-9), CAPES (grant 88881.313535/201901), CNPq (grant 312458/2020-7), and the Alexander von Humboldt Foundation. For the publication fee we acknowledge financial support by Deutsche Forschungsgemeinschaft (DFG) within the funding programme, Open Access Publikationskosten"as well as by Heidelberg University.

ACKNOWLEDGMENTS

We kindly acknowledge the captain and crew of R/V METEOR during research cruise M125. Further, we thank Bernd Knape for assistance in ICP-MS measurements, Oliver A. Kern, Laurin S. Kolb and Maria Wierzbicka-Wieczorek for scientific discussion, Julia Hoffmann and Barbara Hennrich for laboratory assistance. Nicole Mantke and Volker Wennrich are thanked for help with XRF analysis, Daniela Warok and Bianca Stapper for assistance in lipid biomarker analysis. We thank Ed Hathorne (editor) and three reviewers for constructive comments on our manuscript.

SUPPLEMENTARY MATERIAL

The Supplementary Material for this article can be found online at: https://www.frontiersin.org/articles/10.3389/fmars.2022.878116/full#supplementary-material

REFERENCES

Alves, E. Q., Macario, K. D., Spotorno, P., Oliveira, F. M., Muniz, M. C., Fallon, S., et al. (2021). Nineteenth-Century Expeditions and the Radiocarbon Marine Reservoir Effect on the Brazilian Coast. *Geochim. Cosmochim. Acta* 297, 276–287. doi: 10.1016/j.gca.2020.11.021

Ambrizzi, T., de Souza, E. B., and Pulwarty, R. S. (2004). "The Hadley and Walker Regional Circulations and Associated ENSO Impacts on South American Seasonal Rainfall," in *The Hadley Circulation: Present, Past and Future Advances in Global Change Research*. Eds. H. F. Diaz and R. S. Bradley (Dordrecht: Springer Netherlands), 203–235. doi: 10.1007/978-1-4020-2944-8_8

Andreoli, R. V., and Kayano, M. T. (2005). ENSO-Related Rainfall Anomalies in South America and Associated Circulation Features During Warm and Cold Pacific Decadal Oscillation Regimes. *Int. J. Climatol.* 25, 2017–2030. doi: 10.1002/joc.1222

Arbuszewski, J. A., deMenocal, P. B., Cléroux, C., Bradtmiller, L., and Mix, A. (2013). Meridional Shifts of the Atlantic Intertropical Convergence Zone Since the Last Glacial Maximum. *Nat. Geosci.* 6, 959–962. doi: 10.1038/ngeo1961

Austermann, J., Mitrovica, J. X., Latychev, K., and Milne, G. A. (2013). Barbados-Based Estimate of Ice Volume at Last Glacial Maximum Affected by Subducted Plate. *Nat. Geosci.* 6, 553–557. doi: 10.1038/ngeo1859

Bahr, A., Doubrawa, M., Titschack, J., Austermann, G., Koutsodendris, A., Nürnberg, D., et al. (2020). Monsoonal Forcing of Cold-Water Coral Growth Off Southeastern Brazil During the Past 160 Kyr. *Biogeosciences* 17, 5883–5908. doi: 10.5194/bg-17-5883-2020

Bahr, A., Hoffmann, J., Schönfeld, J., Schmidt, M. W., Nürnberg, D., Batenburg, S. J., et al. (2018). Low-Latitude Expressions of High-Latitude Forcing During Heinrich Stadial 1 and the Younger Dryas in Northern South America. *Global Planet. Change* 160, 1–9. doi: 10.1016/j.gloplacha.2017.11.008

Bahr, A., Kaboth-Bahr, S., Jaeschke, A., Chiessi, C., Cruz, F., Carvalho, L., et al. (2021). Late Holocene Precipitation Fluctuations in South America Triggered by Variability of the North Atlantic Overturning Circulation. *Paleoceanogr. Paleoclimatol.* 36, e2021PA004223. doi: 10.1029/2021PA004223

Bahr, A., Spadano Albuquerque, A. L., Ardenghi, N., Batenburg, S., Bayer, M., Catunda, M. C., et al. (2016). *South American Hydrological Balance and Paleoceanography During the Late Pleistocene and Holocene (SAMBA) - Cruise No. M125 - March 21 - April 15, 2016 - Rio De Janeiro (Brazil) - Fortaleza (Brazil)* (Bremen: DFG-Senatskommission für Ozeanographie). doi: 10.2312/cr_m125

Baker, P. A., Rigsby, C. A., Seltzer, G. O., Fritz, S. C., Lowenstein, T. K., Bacher, N. P., et al. (2001). Tropical Climate Changes at Millennial and Orbital Timescales on the Bolivian Altiplano. *Nature* 409, 698–701. doi: 10.1038/35055524

Barker, S., and Diz, P. (2014). Timing of the Descent Into the Last Ice Age Determined by the Bipolar Seesaw. *Paleoceanography* 29, 489–507. doi: 10.1002/2014PA002623

Barker, S., Diz, P., Vautravers, M. J., Pike, J., Knorr, G., Hall, I. R., et al. (2009). Interhemispheric Atlantic Seesaw Response During the Last Deglaciation. *Nature* 457, 1097–1102. doi: 10.1038/nature07770

Behling, H. (1997). Late Quaternary Vegetation, Climate and Fire History From the Tropical Mountain Region of Morro De Itapeva, SE Brazil. *Palaeogeogr. Palaeoclimatol. Palaeoecol.* 129, 407–422. doi: 10.1016/S0031-0182(97)88177-1

Behling, H. (2002). South and Southeast Brazilian Grasslands During Late Quaternary Times: A Synthesis. *Palaeogeogr. Palaeoclimatol. Palaeoecol.* 177, 19–27. doi: 10.1016/S0031-0182(01)00349-2

Bernal, J. P., Cruz, F. W., Stríkis, N. M., Wang, X., Deininger, M., Catunda, M. C. A., et al. (2016). High-Resolution Holocene South American Monsoon History Recorded by a Speleothem From Botuverá Cave, Brazil. *Earth Planet. Sci. Lett.* 450, 186–196. doi: 10.1016/j.epsl.2016.06.008

Biscaye, P. E. (1965). Mineralogy and Sedimentation of Recent Deep-Sea Clay in the Atlantic Ocean and Adjacent Seas and Oceans. *Geol. Soc. America Bull.* 76, 803. doi: 10.1130/0016-7606(1965)76[803:MASORD]2.0.CO;2

Blaauw, M., and Christen, J. A. (2011). Flexible Paleoclimate Age-Depth Models Using an Autoregressive Gamma Process. *Bayes. Anal.* 6, 457–474. doi: 10.1214/11-BA618

Blunier, T., Schwander, J., Stauffer, B., Stocker, T., Dällenbach, A., Indermühle, A., et al. (1997). Timing of the Antarctic Cold Reversal and the Atmospheric CO2 Increase With Respect to the Younger Dryas Event. *Geophys. Res. Lett.* 24, 2683–2686. doi: 10.1029/97GL02658

Boers, N., Rheinwalt, A., Bookhagen, B., Barbosa, H. M. J., Marwan, N., Marengo, J., et al. (2014). The South American Rainfall Dipole: A Complex Network Analysis of Extreme Events. *Geophys. Res. Lett.* 41, 7397–7405. doi: 10.1002/2014GL061829

Böhm, E., Lippold, J., Gutjahr, M., Frank, M., Blaser, P., Antz, B., et al. (2015). Strong and Deep Atlantic Meridional Overturning Circulation During the Last Glacial Cycle. *Nature* 517, 73–76. doi: 10.1038/nature14059

Bonatti, E., and Gartner, S. (1973). Caribbean Climate During Pleistocene Ice Ages. *Nature* 244, 563–565. doi: 10.1038/244563a0

Brendryen, J., Haflidason, H., Yokoyama, Y., Haaga, K. A., and Hannisdal, B. (2020). Eurasian Ice Sheet Collapse was a Major Source of Meltwater Pulse 1A 14,600 Years Ago. *Nat. Geosci.* 13, 363–368. doi: 10.1038/s41561-020-0567-4

Broecker, W. S. (1998). Paleocean Circulation During the Last Deglaciation: A Bipolar Seesaw? *Paleoceanography* 13, 119–121. doi: 10.1029/97PA03707

Burnett, A. P., Soreghan, M. J., Scholz, C. A., and Brown, E. T. (2011). Tropical East African Climate Change and its Relation to Global Climate: A Record From Lake Tanganyika, Tropical East Africa, Over the Past 90+Kyr.

Palaeogeogr. Palaeoclimatol. Palaeoecol. 303, 155–167. doi: 10.1016/j.palaeo.2010.02.011

Campos, M. C., Chiessi, C. M., Prange, M., Mulitza, S., Kuhnert, H., Paul, A., et al. (2019). A New Mechanism for Millennial Scale Positive Precipitation Anomalies Over Tropical South America. *Quaternary. Sci. Rev.* 225, 105990. doi: 10.1016/j.quascirev.2019.105990

Carvalho, L. M. V., Jones, C., and Liebmann, B. (2004). The South Atlantic Convergence Zone: Intensity, Form, Persistence, and Relationships With Intraseasonal to Interannual Activity and Extreme Rainfall. *J. Climate* 17, 88–108. doi: 10.1175/1520-0442(2004)017<0088:TSACZI>2.0.CO;2

Ceppi, P., Hwang, Y.-T., Liu, X., Frierson, D. M. W., and Hartmann, D. L. (2013). The Relationship Between the ITCZ and the Southern Hemispheric Eddy-Driven Jet. *J. Geophys. Res.: Atmosph.* 118, 5136–5146. doi: 10.1002/jgrd.50461

Chaves, R. R., and Nobre, P. (2004). Interactions Between Sea Surface Temperature Over the South Atlantic Ocean and the South Atlantic Convergence Zone. *Geophys. Res. Lett.* 31. doi: 10.1029/2003GL018647

Chiessi, C. M., Mulitza, S., Mollenhauer, G., Silva, J. B., Groeneveld, J., and Prange, M. (2015). Thermal Evolution of the Western South Atlantic and the Adjacent Continent During Termination 1. *Climate Past.* 11, 915–929. doi: 10.5194/cp-11-915-2015

Chiessi, C. M., Mulitza, S., Pätzold, J., and Wefer, G. (2010). How Different Proxies Record Precipitation Variability Over Southeastern South America. *IOP. Conf. Ser.: Earth Environ. Sci.* 9, 12007. doi: 10.1088/1755-1315/9/1/012007

Chiessi, C. M., Mulitza, S., Paul, A., Pätzold, J., Groeneveld, J., and Wefer, G. (2008). South Atlantic Interocean Exchange as the Trigger for the Bølling Warm Event. *Geology* 36, 919. doi: 10.1130/G24979A.1

Chiessi, C. M., Ulrich, S., Mulitza, S., Pätzold, J., and Wefer, G. (2007). Signature of the Brazil-Malvinas Confluence (Argentine Basin) in the Isotopic Composition of Planktonic Foraminifera From Surface Sediments. *Mar. Micropaleontol.* 64, 52–66. doi: 10.1016/j.marmicro.2007.02.002

Christen, J. A., and Pérez, S. (2009). A New Robust Statistical Model for Radiocarbon Data. *Radiocarbon* 51, 1047–1059. doi: 10.1017/S003382220003410X

Clift, P. D., Wan, S., and Blusztajn, J. (2014). Reconstructing Chemical Weathering, Physical Erosion and Monsoon Intensity Since 25Ma in the Northern South China Sea: A Review of Competing Proxies. *Earth-Sci. Rev.* 130, 86–102. doi: 10.1016/j.earscirev.2014.01.002

Coelho, C. A. S., de Oliveira, C. P., Ambrizzi, T., Reboita, M. S., Carpenedo, C. B., Campos, J. L. P. S., et al. (2016). The 2014 Southeast Brazil Austral Summer Drought: Regional Scale Mechanisms and Teleconnections. *Clim. Dyn.* 46, 3737–3752. doi: 10.1007/s00382-015-2800-1

Coumou, D., Lehmann, J., and Beckmann, J. (2015). The Weakening Summer Circulation in the Northern Hemisphere Mid-Latitudes. *Science* 348, 324–327. doi: 10.1126/science.1261768

Coumou, D., Petoukhov, V., Rahmstorf, S., Petri, S., and Schellnhuber, H. J. (2014). Quasi-Resonant Circulation Regimes and Hemispheric Synchronization of Extreme Weather in Boreal Summer. *Proc. Natl. Acad. Sci.* 111, 12331–12336. doi: 10.1073/pnas.1412797111

I. W. Croudace and R. G. Rothwell (Eds.) (2015). "Micro-XRF Studies of Sediment Cores," in *Applications of a non-Destructive Tool for the Environmental Sciences* (Dordrecht: Springer Netherlands). doi: 10.1007/978-94-017-9849-5

Cruz, F. W., Burns, S. J., Jercinovic, M., Karmann, I., Sharp, W. D., and Vuille, M. (2007). Evidence of Rainfall Variations in Southern Brazil From Trace Element Ratios (Mg/Ca and Sr/Ca) in a Late Pleistocene Stalagmite. *Geochim. Cosmochim. Acta* 71, 2250–2263. doi: 10.1016/j.gca.2007.02.005

Cruz, F. W., Burns, S. J., Karmann, I., Sharp, W. D., and Vuille, M. (2006). Reconstruction of Regional Atmospheric Circulation Features During the Late Pleistocene in Subtropical Brazil From Oxygen Isotope Composition of Speleothems. *Earth Planet. Sci. Lett.* 248, 495–507. doi: 10.1016/j.epsl.2006.06.019

Cruz, F. W., Burns, S. J., Karmann, I., Sharp, W. D., Vuille, M., Cardoso, A. O., et al. (2005). Insolation-Driven Changes in Atmospheric Circulation Over the Past 116,000 Years in Subtropical Brazil. *Nature* 434, 63–66. doi: 10.1038/nature03365

Deplazes, G., Lückge, A., Peterson, L. C., Timmermann, A., Hamann, Y., Hughen, K. A., et al. (2013). Links Between Tropical Rainfall and North Atlantic Climate During the Last Glacial Period. *Nat. Geosci.* 6, 213–217. doi: 10.1038/ngeo1712

Díaz, A., and Aceituno, P. (2003). Atmospheric Circulation Anomalies During Episodes of Enhanced and Reduced Convective Cloudiness Over Uruguay. *J. Climate* 16, 3171–3185. doi: 10.1175/1520-0442(2003)016<3171:ACADEO>2.0.CO;2

Donohoe, A., Marshall, J., Ferreira, D., and Mcgee, D. (2012). The Relationship Between ITCZ Location and Cross-Equatorial Atmospheric Heat Transport: From the Seasonal Cycle to the Last Glacial Maximum. *J. Climate* 26, 3597–3618. doi: 10.1175/JCLI-D-12-00467.1

Doyle, M. E., and Barros, V. R. (2002). Midsummer Low-Level Circulation and Precipitation in Subtropical South America and Related Sea Surface Temperature Anomalies in the South Atlantic. *J. Climate* 15, 3394–3410. doi: 10.1175/1520-0442(2002)015<3394:MLLCAP>2.0.CO;2

Elderfield, H., Vautravers, M., and Cooper, M. (2002). The Relationship Between Shell Size and Mg/Ca, Sr/Ca, δ18o, and δ13c of Species of Planktonic Foraminifera. *Geochem. Geophys. Geosyst.* 3, 1–13. doi: 10.1029/2001GC000194

Fleitmann, D., Treble, P., Cruz, F.Jr., Cole, J., and Cobb, K. (2008). "White Paper on "Speleothem-Based Climate Proxy Records"," in *PAGES/CLIVAR Paleoclimate Uncertainties Workshop Report (Citeseer)*. (International Center for Theoretical Physics, Trieste, Italy: PAGES/CLIVAR Paleoclimate Uncertainties Workshop) Available at: https://pastglobalchanges.org/sites/default/files/download/docs/meeting-products/other/2008-trieste-ws-whitepaper-speleothems.pdf (accessed on 13 June 2022).

Freeman, K. H., and Colarusso, L. A. (2001). Molecular and Isotopic Records of C4 Grassland Expansion in the Late Miocene. *Geochim. Cosmochim. Acta* 65, 1439–1454. doi: 10.1016/S0016-7037(00)00573-1

Freeman, K. H., and Pancost, R. D. (2014). ""12.15 - Biomarkers for Terrestrial Plants and Climate,"," in *Treatise on Geochemistry, 2nd ed.* Eds. H. D. Holland and K. K. Turekian (Oxford: Elsevier), 395–416. doi: 10.1016/B978-0-08-095975-7.01028-7

Friedrich, O., Schiebel, R., Wilson, P. A., Weldeab, S., Beer, C. J., Cooper, M. J., et al. (2012). Influence of Test Size, Water Depth, and Ecology on Mg/Ca, Sr/Ca, δ18o and δ13c in Nine Modern Species of Planktic Foraminifers. *Earth Planet. Sci. Lett.* 319–320, 133–145. doi: 10.1016/j.epsl.2011.12.002

Gan, M. A., Kousky, V. E., and Ropelewski, C. F. (2004). The South America Monsoon Circulation and Its Relationship to Rainfall Over West-Central Brazil. *J. Climate* 17, 47–66. doi: 10.1175/1520-0442(2004)017<0047:TSAMCA>2.0.CO;2

Gan, M. A., and Rao, V. B. (1991). Surface Cyclogenesis Over South America. *Month. Weath. Rev.* 119, 1293–1302. doi: 10.1175/1520-0493(1991)119<1293:SCOSA>2.0.CO;2

Garreaud, R. D., Vuille, M., Compagnucci, R., and Marengo, J. (2009). Present-Day South American Climate. *Palaeogeogr. Palaeoclimatol. Palaeoecol.* 281, 180–195. doi: 10.1016/j.palaeo.2007.10.032

Gelbrecht, M., Boers, N., and Kurths, J. (2018). Phase Coherence Between Precipitation in South America and Rossby Waves. *Sci. Adv.* 4, eaau3191. doi: 10.1126/sciadv.aau3191

Gonzalez, P. L. M., Goddard, L., and Greene, A. M. (2013). Twentieth-Century Summer Precipitation in South Eastern South America: Comparison of Gridded and Station Data. *Int. J. Climatol.* 33, 2923–2928. doi: 10.1002/joc.3633

Govin, A., Holzwarth, U., Heslop, D., Keeling, L. F., Zabel, M., Mulitza, S., et al. (2012). Distribution of Major Elements in Atlantic Surface Sediments (36°N–49°S): Imprint of Terrigenous Input and Continental Weathering. *Geochem. Geophys. Geosyst.* 13. doi: 10.1029/2011GC003785

Grimm, A. M. (2011). Interannual Climate Variability in South America: Impacts on Seasonal Precipitation, Extreme Events, and Possible Effects of Climate Change. *Stoch. Environ. Res. Risk Assess.* 25, 537–554. doi: 10.1007/s00477-010-0420-1

Grimm, A. M., and Ambrizzi, T. (2009). "Teleconnections Into South America From the Tropics and Extratropics on Interannual and Intraseasonal Timescales in Past Climate Variability in South America and Surrounding Regions," in *From the Last Glacial Maximum to the Holocene Developments in Paleoenvironmental Research*. Eds. F. Vimeux, F. Sylvestre and M. Khodri (Dordrecht: Springer Netherlands), 159–191. doi: 10.1007/978-90-481-2672-9_7

Grimm, A. M., and Saboia, J. P. J. (2015). Interdecadal Variability of the South American Precipitation in the Monsoon Season. *J. Climate* 28, 755–775. doi: 10.1175/JCLI-D-14-00046.1

Gu, F., Chiessi, C. M., Zonneveld, K. A. F., and Behling, H. (2018). Late Quaternary Environmental Dynamics Inferred From Marine Sediment Core GeoB6211-2 Off Southern Brazil. *Palaeogeogr. Palaeoclimatol. Palaeoecol.* 496, 48–61. doi: 10.1016/j.palaeo.2018.01.015

Gu, F., Pätzold, J., and Behling, H. (2020). Evidence of Cooling in the Tropical South Atlantic Off Southeastern Brazil During the Last 50 Kyr. *Rev. Palaeobot. Palynol.* 272, 104128. doi: 10.1016/j.revpalbo.2019.104128

Gu, F., Zonneveld, K. A. F., Chiessi, C. M., Arz, H. W., Pätzold, J., and Behling, H. (2017). Long-Term Vegetation, Climate and Ocean Dynamics Inferred From a 73,500 Years Old Marine Sediment Core (GeoB2107-3) Off Southern Brazil. *Quaternary. Sci. Rev.* 172, 55–71. doi: 10.1016/j.quascirev.2017.06.028

Heaton, T. J., Köhler, P., Butzin, M., Bard, E., Reimer, R. W., Austin, W. E. N., et al. (2020). Marine20—The Marine Radiocarbon Age Calibration Curve (0–55,000 Cal BP). *Radiocarbon* 62, 779–820. doi: 10.1017/RDC.2020.68

Herbert, T. D. (2014). "Alkenone Paleotemperature Determinations," in *Treatise on Geochemistry* (Oxford: Elsevier), 399–433. doi: 10.1016/B978-0-08-095975-7.00615-X

Hopmans, E. C., Schouten, S., and Sinninghe Damsté, J. S. (2016). The Effect of Improved Chromatography on GDGT-Based Palaeoproxies. *Org. Geochem.* 93, 1–6. doi: 10.1016/j.orggeochem.2015.12.006

Hopmans, E. C., Weijers, J. W. H., Schefuß, E., Herfort, L., Sinninghe Damsté, J. S., and Schouten, S. (2004). A Novel Proxy for Terrestrial Organic Matter in Sediments Based on Branched and Isoprenoid Tetraether Lipids. *Earth Planet. Sci. Lett.* 224, 107–116. doi: 10.1016/j.epsl.2004.05.012

Hou, A., Bahr, A., Raddatz, J., Voigt, S., Greule, M., Albuquerque, A. L., et al. (2020). Insolation and Greenhouse Gas Forcing of the South American Monsoon System Across Three Glacial-Interglacial Cycles. *Geophys. Res. Lett.* 47, e2020GL087948. doi: 10.1029/2020GL087948

Huang, Y., Bol, R., Harkness, D. D., Ineson, P., and Eglinton, G. (1996). Post-Glacial Variations in Distributions, 13C and 14C Contents of Aliphatic Hydrocarbons and Bulk Organic Matter in Three Types of British Acid Upland Soils. *Org. Geochem.* 24, 273–287. doi: 10.1016/0146-6380(96)00039-3

Huguet, C., Hopmans, E. C., Febo-Ayala, W., Thompson, D. H., Sinninghe Damsté, J. S., and Schouten, S. (2006). An Improved Method to Determine the Absolute Abundance of Glycerol Dibiphytanyl Glycerol Tetraether Lipids. *Org. Geochem.* 37, 1036–1041. doi: 10.1016/j.orggeochem.2006.05.008

Huguet, C., Smittenberg, R. H., Boer, W., Sinninghe Damsté, J. S., and Schouten, S. (2007). Twentieth Century Proxy Records of Temperature and Soil Organic Matter Input in the Drammensfjord, Southern Norway. *Org. Geochem.* 38, 1838–1849. doi: 10.1016/j.orggeochem.2007.06.015

Jaeschke, A., Wengler, M., Hefter, J., Ronge, T. A., Geibert, W., Mollenhauer, G., et al. (2017). A Biomarker Perspective on Dust, Productivity, and Sea Surface Temperature in the Pacific Sector of the Southern Ocean. *Geochim. Cosmochim. Acta* 204, 120–139. doi: 10.1016/j.gca.2017.01.045

Jones, C., and Carvalho, L. M. V. (2018). The Influence of the Atlantic Multidecadal Oscillation on the Eastern Andes Low-Level Jet and Precipitation in South America. *NPJ Clim. Atmos. Sci.* 1, 1–7. doi: 10.1038/s41612-018-0050-8

Junquas, C., Vera, C. S., Li, L., and Le Treut, H. (2013). Impact of Projected SST Changes on Summer Rainfall in Southeastern South America. *Clim. Dyn.* 40, 1569–1589. doi: 10.1007/s00382-013-1695-y

Kanner, L. C., Burns, S. J., Cheng, H., and Edwards, R. L. (2012). High-Latitude Forcing of the South American Summer Monsoon During the Last Glacial. *Science* 335, 570–573. doi: 10.1126/science.1213397

Karner, M. B., DeLong, E. F., and Karl, D. M. (2001). Archaeal Dominance in the Mesopelagic Zone of the Pacific Ocean. *Nature* 409, 507–510. doi: 10.1038/35054051

Kirst, G. J., Schneider, R. R., Müller, P. J., von Storch, I., and Wefer, G. (1999). Late Quaternary Temperature Variability in the Benguela Current System Derived From Alkenones. *Quaternary. Res.* 52, 92–103. doi: 10.1006/qres.1999.2040

Lantzsch, H., Hanebuth, T. J. J., Chiessi, C. M., Schwenk, T., and Violante, R. A. (2014). The High-Supply, Current-Dominated Continental Margin of Southeastern South America During the Late Quaternary. *Quaternary. Res.* 81, 339–354. doi: 10.1016/j.yqres.2014.01.003

Lee, S.-Y., Chiang, J. C. H., Matsumoto, K., and Tokos, K. S. (2011). Southern Ocean Wind Response to North Atlantic Cooling and the Rise in Atmospheric CO2: Modeling Perspective and Paleoceanographic Implications. *Paleoceanography* 26. doi: 10.1029/2010PA002004

Liebmann, B., Kiladis, G. N., Marengo, J., Ambrizzi, T., and Glick, J. D. (1999). Submonthly Convective Variability Over South America and the South Atlantic Convergence Zone. *J. Climate* 12, 1877–1891. doi: 10.1175/1520-0442(1999)012<1877:SCVOSA>2.0.CO;2

Liebmann, B., Kiladis, G. N., Vera, C. S., Saulo, A. C., and Carvalho, L. M. V. (2004). Subseasonal Variations of Rainfall in South America in the Vicinity of the Low-Level Jet East of the Andes and Comparison to Those in the South Atlantic Convergence Zone. *J. Climate* 17, 3829–3842. doi: 10.1175/1520-0442(2004)017<3829:SVORIS>2.0.CO;2

Lippold, J., Pöppelmeier, F., Süfke, F., Gutjahr, M., Goepfert, T. J., Blaser, P., et al. (2019). Constraining the Variability of the Atlantic Meridional Overturning Circulation During the Holocene. *Geophys. Res. Lett.* 46, 11338–11346. doi: 10.1029/2019GL084988

Liu, J., Milne, G. A., Kopp, R. E., Clark, P. U., and Shennan, I. (2016). Sea-Level Constraints on the Amplitude and Source Distribution of Meltwater Pulse 1a. *Nat. Geosci.* 9, 130–134. doi: 10.1038/ngeo2616

Maksic, J., Venancio, I. M., Shimizu, M. H., Chiessi, C. M., Piacsek, P., Sampaio, G., et al. (2022). Brazilian Biomes Distribution: Past and Future. *Palaeogeogr. Palaeoclimatol. Palaeoecol.* 585, 110717. doi: 10.1016/j.palaeo.2021.110717

Mann, M. E., Rahmstorf, S., Kornhuber, K., Steinman, B. A., Miller, S. K., and Coumou, D. (2017). Influence of Anthropogenic Climate Change on Planetary Wave Resonance and Extreme Weather Events. *Sci. Rep.* 7, 45242. doi: 10.1038/srep45242

Marengo, J. A., Soares, W. R., Saulo, C., and Nicolini, M. (2004). Climatology of the Low-Level Jet East of the Andes as Derived From the NCEP–NCAR Reanalyses: Characteristics and Temporal Variability. *J. Climate* 17, 2261–2280. doi: 10.1175/1520-0442(2004)017<2261:COTLJE>2.0.CO;2

Marengo, J. A., Torres, R. R., and Alves, L. M. (2017). Drought in Northeast Brazil—past, Present, and Future. *Theor. Appl. Climatol.* 129, 1189–1200. doi: 10.1007/s00704-016-1840-8

Masson-Delmotte, V., Zhai, P., Pirani, A., Connors, S. L., Péan, C., Berger, S., et al. (2021). "Ipc: Climate Change 2021: The Physical Science Basis," in *Contribution of Working Group I to the Sixth Assessment Report of the Intergovernmental Panel on Climate Change* (Cambridge, United Kingdom and New York, NY, USA: Cambridge University Press).

Mathias, G. L., Roud, S. C., Chiessi, C. M., Campos, M. C., Dias, B. B., Santos, T. P., et al. (2021). A Multi-Proxy Approach to Unravel Late Pleistocene Sediment Flux and Bottom Water Conditions in the Western South Atlantic Ocean. *Paleoceanogr. Paleoclimatol.* 36, e2020PA004058. doi: 10.1029/2020PA004058

McGee, D., Donohoe, A., Marshall, J., and Ferreira, D. (2014). Changes in ITCZ Location and Cross-Equatorial Heat Transport at the Last Glacial Maximum, Heinrich Stadial 1, and the Mid-Holocene. *Earth Planet. Sci. Lett.* 390, 69–79. doi: 10.1016/j.epsl.2013.12.043

McManus, J. F., Francois, R., Gherardi, J.-M., Keigwin, L. D., and Brown-Leger, S. (2004). Collapse and Rapid Resumption of Atlantic Meridional Circulation Linked to Deglacial Climate Changes. *Nature* 428, 834–837. doi: 10.1038/nature02494

Meier, K. J. F., Bahr, A., Chiessi, C. M., Albuquerque, A. L., Raddatz, J., and Friedrich, O. (2021). Role of the Tropical Atlantic for the Interhemispheric Heat Transport During the Last Deglaciation. *Paleoceanogr. Paleoclimatol.* 36, e2020PA004107. doi: 10.1029/2020PA004107

Moura, A. D., and Shukla, J. (1981). On the Dynamics of Droughts in Northeast Brazil: Observations, Theory and Numerical Experiments With a General Circulation Model. *J. Atmosph. Sci.* 38, 2653–2675. doi: 10.1175/1520-0469(1981)038<2653:OTDODI>2.0.CO;2

Mulitza, S., Chiessi, C. M., Schefuß, E., Lippold, J., Wichmann, D., Antz, B., et al. (2017). Synchronous and Proportional Deglacial Changes in Atlantic Meridional Overturning and Northeast Brazilian Precipitation: AMOC and Precipitation Over NE Brazil. *Paleoceanography* 32, 622–633. doi: 10.1002/2017PA003084

Nogués-Paegle, J., and Mo, K. C. (1997). Alternating Wet and Dry Conditions Over South America During Summer. *Month. Weath. Rev.* 125, 279–291. doi: 10.1175/1520-0493(1997)125<0279:AWADCO>2.0.CO;2

Novello, V. F., Cruz, F. W., McGlue, M. M., Wong, C. I., Ward, B. M., Vuille, M., et al. (2019). Vegetation and Environmental Changes in Tropical South America From the Last Glacial to the Holocene Documented by Multiple Cave Sediment Proxies. *Earth Planet. Sci. Lett.* 524, 115717. doi: 10.1016/j.epsl.2019.115717

Novello, V. F., Cruz, F. W., Vuille, M., Stríkis, N. M., Edwards, R. L., Cheng, H., et al. (2017). A High-Resolution History of the South American Monsoon From Last Glacial Maximum to the Holocene. *Sci. Rep.* 7, 44267. doi: 10.1038/srep44267

Pedro, J. B., Bostock, H. C., Bitz, C. M., He, F., Vandergoes, M. J., Steig, E. J., et al. (2016). The Spatial Extent and Dynamics of the Antarctic Cold Reversal. *Nat. Geosci.* 9, 51–55. doi: 10.1038/ngeo2580

Pedro, J. B., van Ommen, T. D., Rasmussen, S. O., Morgan, V. I., Chappellaz, J., Moy, A. D., et al. (2011). The Last Deglaciation: Timing the Bipolar Seesaw. *Climate Past.* 7, 671–683. doi: 10.5194/cp-7-671-2011

Peterson, R. G., and Stramma, L. (1991). Upper-Level Circulation in the South Atlantic Ocean. *Prog. Oceanogr.* 26, 1–73. doi: 10.1016/0079-6611(91)90006-8

Portilho-Ramos, R. C., Chiessi, C. M., Zhang, Y., Mulitza, S., Kucera, M., Siccha, M., et al. (2017). Coupling of Equatorial Atlantic Surface Stratification to Glacial Shifts in the Tropical Rainbelt. *Sci. Rep.* 7, 1561. doi: 10.1038/s41598-017-01629-z

Prahl, F. G., Collier, R. B., Dymond, J., Lyle, M., and Sparrow, M. A. (1993). A Biomarker Perspective on Prymnesiophyte Productivity in the Northeast Pacific Ocean. *Deep. Sea. Res. Part I.: Oceanogr. Res. Pap.* 40, 2061–2076. doi: 10.1016/0967-0637(93)90045-5

Ramos, A. M., Blamey, R. C., Algarra, I., Nieto, R., Gimeno, L., Tomé, R., et al. (2019). From Amazonia to Southern Africa: Atmospheric Moisture Transport Through Low-Level Jets and Atmospheric Rivers. *Ann. New York. Acad. Sci.* 1436, 217–230. doi: 10.1111/nyas.13960

Rao, V. B., de Lima, M. C., and Franchito, S. H. (1993). Seasonal and Interannual Variations of Rainfall Over Eastern Northeast Brazil. *J. Climate* 6, 1754–1763. doi: 10.1175/1520-0442(1993)006<1754:SAIVOR>2.0.CO;2

Ravelo, A. C., and Hillaire-Marcel, C. (2007). ""Chapter Eighteen The Use of Oxygen and Carbon Isotopes of Foraminifera in Paleoceanography,"," in *Developments in Marine Geology* (Amsterdam: Elsevier), 735–764. doi: 10.1016/S1572-5480(07)01023-8

Riedinger, N., Pfeifer, K., Kasten, S., Garming, J. F. L., Vogt, C., and Hensen, C. (2005). Diagenetic Alteration of Magnetic Signals by Anaerobic Oxidation of Methane Related to a Change in Sedimentation Rate. *Geochim. Cosmochim. Acta* 69, 4117–4126. doi: 10.1016/j.gca.2005.02.004

Rippert, N., Nürnberg, D., Raddatz, J., Maier, E., Hathorne, E., Bijma, J., et al. (2016). Constraining Foraminiferal Calcification Depths in the Western Pacific Warm Pool. *Mar. Micropaleontol.* 128, 14–27. doi: 10.1016/j.marmicro.2016.08.004

Robertson, A. W., and Mechoso, C. R. (2000). Interannual and Interdecadal Variability of the South Atlantic Convergence Zone. *Month. Weath. Rev.* 128, 2947–2957. doi: 10.1175/1520-0493(2000)128<2947:IAIVOT>2.0.CO;2

Rostek, F., Bard, E., Beaufort, L., Sonzogni, C., and Ganssen, G. (1997). Sea Surface Temperature and Productivity Records for the Past 240 Kyr in the Arabian Sea. *Deep. Sea. Res. Part II.: Top. Stud. Oceanogr.* 44, 1461–1480. doi: 10.1016/S0967-0645(97)00008-8

Salio, P., and Nicolini, M. (2006). "Seasonal Characterization on the Diurnal Cycle of Convection Frequency Over Southeastern South America Under Different Low-Jet Conditions," in *Proceedings of the 8th International Conference on Southern Hemisphere Meteorology and Oceanography.* (Foz do Iguacu, Brazil: 8th International Conference on Southern Hemisphere Meteorology and Oceanography (8ICSHMO)) 1157–1162.

Salio, P., Nicolini, M., and Saulo, A. C. (2002). Chaco Low-Level Jet Events Characterization During the Austral Summer Season. *J. Geophys. Res.: Atmosph.* 107, ACL 32–1-ACL 32-17. doi: 10.1029/2001JD001315

Saulo, A. C., Nicolini, M., and Chou, S. C. (2000). Model Characterization of the South American Low-Level Flow During the 1997–1998 Spring–Summer Season. *Climate Dyn.* 16, 867–881. doi: 10.1007/s003820000085

Saulo, A. C., Seluchi, M. E., and Nicolini, M. (2004). A Case Study of a Chaco Low-Level Jet Event. *Month. Weath. Rev.* 132, 2669–2683. doi: 10.1175/MWR2815.1

Saurral, R. I., Camilloni, I. A., and Barros, V. R. (2017). Low-Frequency Variability and Trends in Centennial Precipitation Stations in Southern South America. *Int. J. Climatol.* 37, 1774–1793. doi: 10.1002/joc.4810

Schneider, T., Bischoff, T., and Haug, G. H. (2014). Migrations and Dynamics of the Intertropical Convergence Zone. *Nature* 513, 45–53. doi: 10.1038/nature13636

Schouten, S., Hopmans, E. C., Pancost, R. D., and Damste, J. S. (2000). Widespread Occurrence of Structurally Diverse Tetraether Membrane Lipids: Evidence for the Ubiquitous Presence of Low-Temperature Relatives of Hyperthermophiles. *Proc. Natl. Acad. Sci.* 97, 14421–14426. doi: 10.1073/pnas.97.26.14421

Silva, V. B. S., and Berbery, E. H. (2006). Intense Rainfall Events Affecting the La Plata Basin. *J. Hydrometeorol.* 7, 769–787. doi: 10.1175/JHM520.1

Sinninghe Damsté, J. S., Rijpstra, W. I. C., Hopmans, E. C., Prahl, F. G., Wakeham, S. G., and Schouten, S. (2002a). Distribution of Membrane Lipids of Planktonic Crenarchaeota in the Arabian Sea. *Appl. Environ. Microbiol.* 68, 2997–3002. doi: 10.1128/AEM.68.6.2997-3002.2002

Sinninghe Damsté, J. S. S., Schouten, S., Hopmans, E. C., van Duin, A. C. T., and Geenevasen, J. A. J. (2002b). Crenarchaeol. *J. Lipid Res.* 43, 1641–1651. doi: 10.1194/jlr.M200148-JLR200

Stocker, T. F. (1998). The Seesaw Effect. *Science* 282, 61–62. doi: 10.1126/science.282.5386.61

Stramma, L., and England, M. (1999). On the Water Masses and Mean Circulation of the South Atlantic Ocean. *J. Geophys. Res.: Ocean.* 104, 20863–20883. doi: 10.1029/1999JC900139

Stríkis, N. M., Chiessi, C. M., Cruz, F. W., Vuille, M., Cheng, H., Barreto, E. A., et al. (2015). Timing and Structure of Mega-SACZ Events During Heinrich Stadial 1. *Geophys. Res. Lett.* 42, 5477–5484A. doi: 10.1002/2015GL064048

Stríkis, N. M., Cruz, F. W., Barreto, E. A. S., Naughton, F., Vuille, M., Cheng, H., et al. (2018). South American Monsoon Response to Iceberg Discharge in the North Atlantic. *Proc. Natl. Acad. Sci.* 115, 3788–3793. doi: 10.1073/pnas.1717784115

Tintelnot, M. (1995). *Transport and Deposition of Fine-Grained Sediments on the Brazilian Continental Shelf as Revealed by Clay Mineral Distribution* (Heidelberg: Univ., Diss.).

Venancio, I. M., Belem, A. L., Santos, T. P., Lessa, D. O., Albuquerque, A. L. S., Mulitza, S., et al. (2017). Calcification Depths of Planktonic Foraminifera From the Southwestern Atlantic Derived From Oxygen Isotope Analyses of Sediment Trap Material. *Mar. Micropaleontol.* 136, 37–50. doi: 10.1016/j.marmicro.2017.08.006

Venancio, I. M., Shimizu, M. H., Santos, T. P., Lessa, D. O., Portilho-Ramos, R. C., Chiessi, C. M., et al. (2020). Changes in Surface Hydrography at the Western Tropical Atlantic During the Younger Dryas. *Global Planet. Change* 184, 103047. doi: 10.1016/j.gloplacha.2019.103047

Venegas, S. A., Mysak, L. A., and Straub, D. N. (1997). Atmosphere–Ocean Coupled Variability in the South Atlantic. *J. Climate* 10, 2904–2920. doi: 10.1175/1520-0442(1997)010<2904:AOCVIT>2.0.CO;2

Vera, C., Baez, J., Douglas, M., Emmanuel, C. B., Marengo, J., Meitin, J., et al. (2006). The South American Low-Level Jet Experiment. *Bull. Am. Meteorol. Soc.* 87, 63–78. doi: 10.1175/BAMS-87-1-63

Vera, C. S., and Díaz, L. (2015). Anthropogenic Influence on Summer Precipitation Trends Over South America in CMIP5 Models. *Int. J. Climatol.* 35, 3172–3177. doi: 10.1002/joc.4153

Vera, C. S., Vigliarolo, P. K., and Berbery, E. H. (2002). Cold Season Synoptic-Scale Waves Over Subtropical South America. *Month. Weath. Rev.* 130, 684–699. doi: 10.1175/1520-0493(2002)130<0684:CSSSWO>2.0.CO;2

Wang, X., Auler, A. S., Edwards, R. L., Cheng, H., Ito, E., Wang, Y., et al. (2007). Millennial-Scale Precipitation Changes in Southern Brazil Over the Past 90,000 Years. *Geophys. Res. Lett.* 34. doi: 10.1029/2007GL031149

Warratz, G., Henrich, R., Voigt, I., Chiessi, C. M., Kuhn, G., and Lantzsch, H. (2017). Deglacial Changes in the Strength of Deep Southern Component Water and Sediment Supply at the Argentine Continental Margin. *Paleoceanography* 32, 796–812. doi: 10.1002/2016PA003079

Weaver, A. J., Saenko, O. A., Clark, P. U., and Mitrovica, J. X. (2003). Meltwater Pulse 1A From Antarctica as a Trigger of the Bølling-Allerød Warm Interval. *Science* 299, 1709–1713. doi: 10.1126/science.1081002

Weijers, J. W. H., Schouten, S., Hopmans, E. C., Geenevasen, J. A. J., David, O. R. P., Coleman, J. M., et al. (2006). Membrane Lipids of Mesophilic Anaerobic Bacteria Thriving in Peats Have Typical Archaeal Traits. *Environ. Microbiol.* 8, 648–657. doi: 10.1111/j.1462-2920.2005.00941.x

Wolf, G., Brayshaw, D. J., Klingaman, N. P., and Czaja, A. (2018). Quasi-Stationary Waves and Their Impact on European Weather and Extreme Events. *Q. J. R. Meteorol. Soc.* 144, 2431–2448. doi: 10.1002/qj.3310

Yarincik, K. M., Murray, R. W., and Peterson, L. C. (2000). Climatically Sensitive Eolian and Hemipelagic Deposition in the Cariaco Basin, Venezuela, Over the

Past 578,000 Years: Results From Al/Ti and K/Al. *Paleoceanography* 15, 210–228. doi: 10.1029/1999PA900048

Zabel, M., Schneider, R. R., Wagner, T., Adegbie, A. T., de Vries, U., and Kolonic, S. (2001). Late Quaternary Climate Changes in Central Africa as Inferred From Terrigenous Input to the Niger Fan. *Quaternary. Res.* 56, 207–217. doi: 10.1006/qres.2001.2261

Zanin, P. R., and Satyamurty, P. (2020). Hydrological Processes Interconnecting the Two Largest Watersheds of South America From Multi-Decadal to Inter-Annual Time Scales: A Critical Review. *Int. J. Climatol.* 40, 4006–4038. doi: 10.1002/joc.6442

Zhang, Y., Chiessi, C. M., Mulitza, S., Sawakuchi, A. O., Häggi, C., Zabel, M., et al. (2017). Different Precipitation Patterns Across Tropical South America During Heinrich and Dansgaard-Oeschger Stadials. *Quaternary. Sci. Rev.* 177, 1–9. doi: 10.1016/j.quascirev.2017.10.012

Zhang, R., and Delworth, T. L. (2005). Simulated Tropical Response to a Substantial Weakening of the Atlantic Thermohaline Circulation. *J. Climate* 18, 1853–1860. doi: 10.1175/JCLI3460.1

Conflict of Interest: The authors declare that the research was conducted in the absence of any commercial or financial relationships that could be construed as a potential conflict of interest.

Publisher's Note: All claims expressed in this article are solely those of the authors and do not necessarily represent those of their affiliated organizations, or those of the publisher, the editors and the reviewers. Any product that may be evaluated in this article, or claim that may be made by its manufacturer, is not guaranteed or endorsed by the publisher.